Fixation and extinction in time-fluctuating spatially structured metapopulations

Matthew Asker [1,*] Mohamed Swailem [2] Uwe C. Täuber [2] and Mauro Mobilia [1,†]

[1]*Department of Applied Mathematics, School of Mathematics, University of Leeds, Leeds LS2 9JT, United Kingdom*

[2]*Department of Physics and Center for Soft Matter and Biological Physics, MC 0435, Robeson Hall, 850 West Campus Drive, Virginia Tech, Blacksburg, Virginia 24061, USA*

(Received 11 April 2025; accepted 14 October 2025; published 21 November 2025)

Bacteria evolve in volatile environments and complex spatial structures. Migration, fluctuations, and environmental variability therefore have a significant impact on the evolution of microbial populations. Here, we consider a class of spatially explicit metapopulation models arranged as regular (circulation) graphs where wild-type and mutant cells compete in a *time-fluctuating* environment in which demes (subpopulations) are connected by slow cell migration. The carrying capacity is the same at each deme and endlessly switches between two values associated with harsh and mild environmental conditions. It is known that environmental variability can lead to population bottlenecks, following which the population is prone to fluctuation-induced extinction. Here, we analyze how slow migration, spatial structure, and fluctuations affect the phenomena of fixation and extinction on clique, cycle, and square lattice metapopulations. When the carrying capacity remains large, bottlenecks are weak and deme extinction can be ignored. The dynamics is thus captured by a coarse-grained description within which the probability and mean time of fixation are obtained analytically. This allows us to show that, in contrast to what happens in static environments, the mutant fixation probability depends on the rate of migration. We also show that the fixation probability and mean fixation time can exhibit a nonmonotonic dependence on the switching rate. When the carrying capacity is small under harsh conditions, bottlenecks are strong, and the metapopulation evolution is shaped by the coupling of deme extinction and strain competition. This yields rich dynamical scenarios, among which we identify the best conditions to eradicate mutants without dooming the metapopulation to extinction. We offer an interpretation of these findings in the context of an idealized treatment strategy and discuss possible generalizations of our models.

DOI: 10.1103/6w4h-8xvk

I. INTRODUCTION

Microbial populations live in volatile and time-varying environments embedded in complex spatial settings, across which the distribution of microbes fluctuates. For instance, many organisms live in densely packed aggregates on surface-attached biofilms [1], numerous commensal bacteria are distributed throughout the gastrointestinal tract [2,3], and patients' organs are spatial environments between which bacteria can migrate [4]. Moreover, natural environments are not static, e.g., temperature, pH, or available resources change over time. These abiotic variations, not caused by the organisms themselves, are referred to as environmental fluctuations and can have a significant influence on the evolution of natural populations. For example, the gut microbiome of a host is exposed to fluctuations of great amplitude on various timescales, and these affect the diversity of the microbiota [5,6]. In small populations, demographic fluctuations are another important form of randomness resulting in fixation—where one strain takes over the community—or extinction [7,8]. Since the variations of population size and composition are often interdependent [9–15], this can lead to the coupling of environmental and demographic fluctuations [16–24]. Their interplay is particularly significant in microbial communities, where it can lead to population bottlenecks, where new colonies consisting of a few cells are prone to fluctuations [25–29]. Population bottlenecks and fluctuations are particularly relevant for the evolution of antimicrobial resistance, when cells surviving antibiotics treatment may replicate leading to the spread of resistance [21,24,30–32].

How likely is a population to be taken over by a mutant or to go extinct? What is the typical time for these events to occur? These are central questions in evolution, and the answers depend on the population's spatial structure as well as the environmental variations and fluctuations. In this context, it is important to understand the impact of spatial structure, migration, and fluctuations on the spread of a mutant strain. A common approach to represent a spatially structured biological population is by dividing it into several demes—well-mixed subpopulations connected by cell migration—hence forming a *metapopulation* [33–42]. The influence of the spatial arrangement of a population and stochastic fluctuations on mutants' fate has been studied in *static* environments both theoretically [33,34,41,43–54] and experimentally [55–58]. Maruyama notably showed that in a

*Contact author: asker@evolbio.mpg.de
†Contact author: M.Mobilia@leeds.ac.uk

constant environment, when cell migration is symmetric and preserves the overall mutant fraction, the fixation probability of a mutant is independent of the spatial structure and migration rate [43]. However, it has been shown that random extinction and recolonization can affect the mutant fixation probability on fully connected (static) graphs, even when cell migration is symmetric [44]. In this case, deme extinction is immediately followed by recolonization by a mixture of cells from other demes [35,36,44]. Furthermore, independent extinction and recolonization by a single neighbor of demes has been studied on fully connected (static) graphs [59]. Recently, the authors of Ref. [41] studied the influence of slow migration on the fate of mutants on static graphs, and demonstrated that migration asymmetry can dramatically affect their fixation probability on certain spatial structures like the star graph. However, the biologically relevant problem of mutants evolving in time-varying spatially structured populations has been rather scarcely investigated, and the case of strains competing to colonize and fixate demes prone to extinction remains underexplored.

Here, we tackle these important issues by studying a class of time-fluctuating microbial metapopulation models consisting of demes in which wild-type and mutant cells evolve in a time-varying environment represented by a switching carrying capacity. We use coarse-grained descriptions of the dynamics to study the joint influence of environmental variability, demographic fluctuations, migration, and spatial structure on the evolution of the metapopulation. We obtain explicit results for cliques (island model [33,34], or fully connected graph), cycles, and two-dimensional grids (with periodic boundaries). In stark contrast with the evolution in static environments, we demonstrate that when bottlenecks are weak, the fixation probability on regular circulation graphs depends on the migration rate. Moreover, we show that under the effect of environmental variability and fluctuations, the fixation probability and mean fixation time can exhibit a nonmonotonic dependence on the switching rate. In the case of strong bottlenecks, arising when the carrying capacity is small under harsh conditions, the dynamics is characterized by deme extinction and strain competition coupled by environmental switching. This yields rich dynamical scenarios among which we identify the best conditions to eradicate mutants without risking metapopulation extinction.

In the next section, we introduce the explicit spatial metapopulation model that we study and outline our methodology. In Sec. III, we present our results in the case of static environments. This paves the way to the detailed analysis in time-fluctuating environments of Sec. IV, with the weak and strong bottleneck regimes, respectively, studied in Secs. IV A and IV B. Section V is dedicated to a discussion of our findings, assumptions, and possible generalizations. We present our conclusions in Sec. VI. Additional technical details are given in a series of Appendixes.

II. MODEL AND METHODS

We consider a class of spatially explicit metapopulation models of Ω demes labeled by $x \in \{1, \ldots, \Omega\}$, each of which at time t consists of a well-mixed subpopulation of n_W cells of wild type W and n_M mutants of strain M. Each wild-type cell has a baseline fitness $f_W = 1$ and all mutant cells have fitness $f_M = 1 + s$. We assume $0 < s \ll 1$, giving M a small selective advantage over W.

The microbial metapopulation can be envisioned as a graph whose nodes $x \in \{1, \ldots, \Omega\}$ are demes (also called sites). Each deme x is a well-mixed subpopulation of size $n(x) = \sum_{\alpha\in\{W,M\}} n_\alpha(x) = n_W(x) + n_M(x)$ located at a node of the metapopulation graph. Thus, $N_{W/M} \equiv \sum_x n_{W/M}(x)$ is the number of W/M individuals across the metapopulation, and $N \equiv N_W + N_M$ is the total number of individuals in the whole graph. Here, we focus on fully connected graphs (as in the island model [33,34]) called cliques, and periodic one- and two-dimensional lattices called, respectively, cycles and grids [see Fig. 1(a)]. These are regular graphs, generally denoted by G = {clique, cycle, grid}, of Ω demes connected by edges to their q_G nearest neighbors via cell migration at per capita rate m (independently from division and death) [33,34,41–43,60] [see Figs. 1(a)–1(c)]. We study the ecoevolutionary dynamics of the metapopulation in the biologically relevant regime of slow migration (whereby intrademe dynamics occur much faster than interdeme dynamics; see below) [41,42,61–63], and consider that initially one deme is occupied entirely by mutants (M deme), while the other $\Omega - 1$ demes (W demes) are all populated by W cells (see Sec. V). All demes are assumed to have the same carrying capacity K that encodes environmental variability. In Sec. III, we assume that K is constant, and in Sec. IV we let the carrying capacity switch endlessly between two values representing mild and harsh conditions [16–24,32]; see below.

In close relation to the Moran process [64–67] (see Appendix B), a reference model in mathematical biology [7], the intrademe dynamics in a deme x is thus represented by a multivariate birth-death process defined by the birth and death of a cell of type $\alpha \in \{W, M\}$ in that site according to the reactions [16,17,22,22,32]

$$n_\alpha \xrightarrow{T_\alpha^+} n_\alpha + 1 \quad \text{and} \quad n_\alpha \xrightarrow{T_\alpha^-} n_\alpha - 1, \tag{1}$$

occurring at the transition rates

$$T_\alpha^+(x) = \frac{f_\alpha}{\overline{f}} n_\alpha \quad \text{and} \quad T_\alpha^-(x) = \frac{n}{K} n_\alpha, \tag{2}$$

where $\overline{f} \equiv (n_W f_W + n_M f_M)/n$ is the average fitness in deme x, and K here denotes the constant carrying capacity in a static environment and its time-switching version in a dynamical environment; see below. In this formulation, without loss of generality, selection operates on birth events. This can be generalized to include selection on deaths (see, e.g., Refs. [10,11].

The interdeme dynamics stems from the migration of one cell of type $\alpha \in \{W, M\}$ from the site x to one of its q_G neighboring demes denoted by y at a per-capita migration rate m. Here, for the sake of simplicity, we assume that the migration rate is the same in all directions and for both types (symmetric migration); see Sec. V for a discussion of these assumptions. The interdeme dynamics for all cells at deme x with its neighboring demes labeled y is therefore implemented according to the reaction

$$[n_\alpha(x), n_\alpha(y)] \xrightarrow{T_\alpha^{m,G}} [n_\alpha(x) - 1, n_\alpha(y) + 1], \tag{3}$$

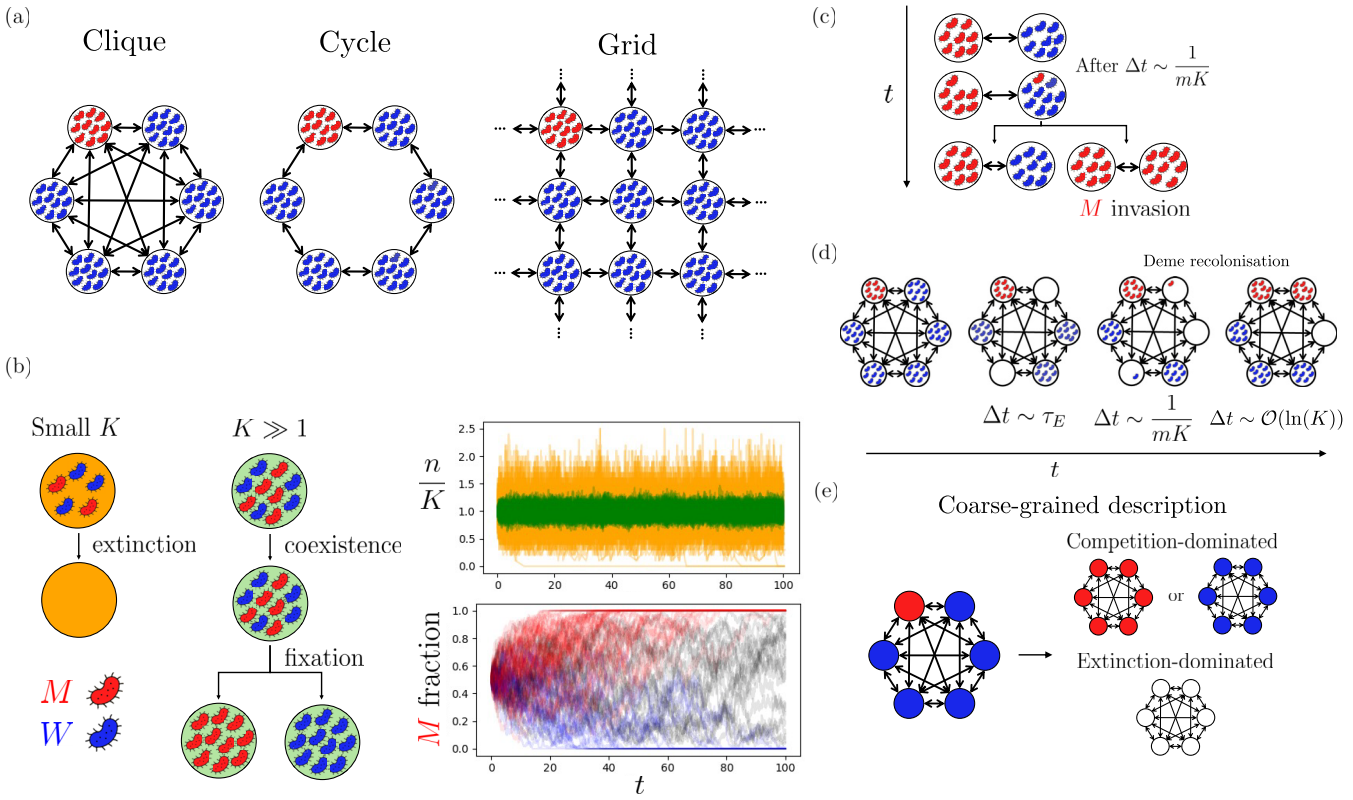

FIG. 1. Metapopulation dynamics in a static environment. (a) Examples of metapopulation graphs: a clique, cycle, and grid (from left to right). Neighboring demes are connected by migration (double arrows). Initially, there is one mutant deme (red/light) and $\Omega - 1$ wild-type demes (blue/dark), and all demes have the same constant carrying capacity K. (b) Dynamics in a single deme. Left: Wild-type W cells (blue/dark) compete with mutants of type M (red/light). When K is small, the deme is prone to extinction. When K is large, both types coexist prior to W or M fixation. Top right: Realizations of the rescaled deme size n/K vs time t for $K = 5$ (orange/light) and $K = 100$ (green/dark) illustrating how n fluctuates about K. Bottom right: Fraction of M cells vs t in a deme with $K = 100$. Deme extinction is not observed. Transient coexistence of W and M is followed by the fixation of W (blue traces) or M (red traces). Here, $s = 0.01$. (c) Invasion of a W deme by an M cell: Any M cell of a deme migrates to a neighboring W site with migration rate m after a mean time $\Delta t = 1/(mK)$, and then type M either quickly fixates, producing an M deme (right), or does not fix leaving the pair of M and W demes unchanged (left). The same picture holds for the invasion of an M deme by a W cell; see text. (d) Deme recolonization (here for the clique): Deme extinction occurs after a mean time τ_E, and empty demes are then recolonized by an invader from a neighboring surviving deme after $\Delta t \sim 1/(mK)$. A recolonized deme is rapidly taken over [in $\Delta t = \mathcal{O}(\ln(K))$]. (e) Coarse-grained description of the metapopulation dynamics: Each deme is always either fully W (blue/dark) or M (red/light) or empty (white). In this description, different scenarios arise, shown for the clique. Competition-dominated regime: All demes are occupied and there is always fixation of W or M. Extinction-dominated regime: There are frequent deme extinctions and the metapopulation quickly goes extinct.

occurring at the migration transition rate

$$T_\alpha^{m,\mathrm{G}}(x) = \frac{m n_\alpha}{q_\mathrm{G}}. \tag{4}$$

On a given metapopulation, if the number of cells migrating into a deme equals the number of cells migrating out, and this is true for all demes, we say that the metapopulation is a circulation. Precisely, the condition here for a metapopulation to be a circulation is given by

$$\sum_{y\ \mathrm{n.n.}\ x} \sum_\alpha T_\alpha^{m,\mathrm{G}}(x) = \sum_{y\ \mathrm{n.n.}\ x} \sum_\alpha T_\alpha^{m,\mathrm{G}}(y) \quad \text{for all } x, \tag{5}$$

where y n.n. x denotes the sum over the q_G neighbors y of the deme x. In our case, this simplifies considerably to give $n(x) = \sum_{y\ \mathrm{n.n.}\ x} n(y)/q_G$ for all x. Intuitively, this means that for our setup, if each deme has the same population size, then the metapopulation is a circulation: There is the same incoming and outgoing migration flow at each deme. This will indeed be the case under sufficiently large carrying capacity.

Microbial communities generally live in time-varying conditions, and are often subject to sudden and drastic environmental changes. Here, environmental variability is encoded in the time variation of the binary carrying capacity [16–24,32]:

$$K(t) = \tfrac{1}{2}[K_- + K_- + \xi(t)(K_+ - K_-)], \tag{6}$$

driven by a random telegraph process $\xi(t) \in \{-1, 1\}$. The colored dichotomous Markov noise (DMN) $\xi(t)$ switches between ± 1 according to $\xi \to -\xi$ at rate ν for the symmetric DMN (see Sec. V and Appendix H for the generalization to asymmetric switching) [69–71]. The carrying capacity, equal across demes, thus switches at a rate ν between a value $K = K_+$ in a mild environment (e.g. abundance of nutrients, lack of toxin) and $K = K_- < K_+$ under harsh environmental conditions (e.g. lack of nutrients, abundance of toxin)

according to $K_- \overset{\nu}{\rightleftharpoons} K_+$, and thus represents random cycles of mild and harsh conditions (feast and famine cycles). The randomly time switching $K(t)$ drives the size of each deme, and is hence responsible for the coupling of demographic fluctuations with environmental variability, an effect particularly important when there are population bottlenecks [16–19,21–24,32]; see below. Here, the DMN is at stationarity, i.e., it is initialized from its long-time distribution where instantaneous correlations become time independent (while the autocovariance is a function of the time difference) [70,72]. This means that the average of the DMN vanishes, $\langle \xi(t) \rangle = 0$, and its autocovariance coincides with its autocorrelation reading $\langle \xi(t)\xi(t') \rangle = e^{-2\nu|t-t'|}$ [69–71], where $\langle \cdot \rangle$ denotes the ensemble average and $1/(2\nu)$ is the finite correlation time (with $t, t' \to \infty$). As a consequence, the fluctuating carrying capacity is always at stationarity, with a constant average $\langle K(t) \rangle = \langle K \rangle = (K_+ + K_-)/2$ and an autocorrelation $\langle K(t)K(t') \rangle = \langle K \rangle e^{-2\nu|t-t'|}$. In our simulations with symmetric random switching, the carrying capacity is initially drawn from its stationary distribution, with $K(0) = K_+$ or $K(0) = K_-$ each with probability $1/2$ (see Sec. V and Appendix H).

The full individual-based model is therefore a continuous-time multivariate Markov process defined by the reactions and transition rates [Eqs. (1)–(4)] that satisfies the master equation (ME) [Eq. (A1)] discussed in Appendix A 1. The microscopic intra- and interdeme dynamics encoded in the ME [Eq. (A1)] has been simulated using the Monte Carlo (MC) method described in Appendix I. The ecoevolutionary dynamics of a single deme is outlined in Appendix A 2. It is worth noting that n, $n_{W/M}$, $T^{\pm}_{W/M}$, and $T^{m,\mathrm{G}}_{W/M}$ are all quantities that depend on the site x and time t, and on ξ in a time-varying environment. However, for notational simplicity, we often drop the explicit dependence on some or all of the variables x, t, and ξ. Below, we combine coarse-grained analytical approximations and individual-based stochastic simulations to study how the spatial structure, migration, and demographic fluctuations influence the fixation and extinction properties of the microbial metapopulation.

III. STATIC ENVIRONMENTS

We first consider a static environment where the carrying capacity K of each deme is constant. In this setting, the size n of each deme rapidly reaches and fluctuates about K, with $n \approx K$ when $K \gg 1$ [see Fig. 1(b), top right]. The expected number of migrants per unit time and deme is thus mK. The occurrence of migration events, alongside the competition between M and W to take over demes of the other type, increases with K. Cell migration and competition are however limited when K is small: Regardless of their type, demes of small size are prone to extinction in a mean time $\tau_E(K)$ [see Figs. 1(b) and 1(d)]. For independent demes of size K, the deme mean extinction time (dMET) $\tau_E(K)$ can be obtained from a logistic birth-death process (see Appendix C) yielding

$$\tau_E(K) \approx \frac{e^K}{K}, \tag{7}$$

when $K \gg 1$ [see Fig. 2(b), top]. We thus refer to K as "small" where fixation of a deme (intrademe dynamics) occurs on slower timescale than its extinction. Similarly, K is referred to as large (i.e., $K \gg 1$) where fixation of a site occurs faster than deme extinction. In our analysis, we distinguish between different dynamical scenarios through

$$\psi(m, K) \equiv mK\tau_E, \tag{8}$$

giving the average number of migration events during the typical deme extinction time. With Eq. (7), we have $\psi(m, K) \approx me^K$ when $K \gg 1$. In the regime where $\psi \gg 1$, many migration events occur before any deme extinction, and the dynamics is thus dominated by M/W competition. When $\psi(m, K) < 1$, migration is ineffective and there is fast extinction of all demes. An intermediate regime where some demes are empty and others occupied by W or M arises when $\psi(m, K) \gtrsim 1$. To rationalize this picture in the coarse-grained description of Ref. [59], it is useful to track the number of occupied demes $j = 0, 1, \ldots, \Omega$ (by either W or M cells). For cliques, as shown in Appendix D, we find that the long-time fraction of occupied demes is

$$\frac{j}{\Omega} \to \frac{\Omega_{\mathrm{occ}}(m, K)}{\Omega} \approx \begin{cases} 1 & \text{if } \psi \gg 1, \\ \frac{\psi - 1}{\psi} & \text{if } \psi \gtrsim 1, \\ 0 & \text{if } \psi < 1. \end{cases} \tag{9}$$

The expression of Ω_{occ} ignores spatial correlations and hence is not accurate for cycles and grids if $\psi(m, K)$ is not much larger than 1. However, $\psi(m, K)$ allows us to efficiently distinguish between the regimes dominated by M/W competition ($\psi \gg 1$) and deme extinction ($\psi < 1$) (see Appendix D). The crossover intermediate regime ($\psi \gtrsim 1$) is discussed in detail in Appendix F.

Henceforth, we refer to "invasion" when a cell of type M/W migrates to and fixates in a W/M deme, and to "recolonization" when a cell of either type migrates into an empty deme and takes it over [see Figs. 1(c) and 1(d)]. The competition-dominated dynamics is characterized by invasions, while the extinction-dominated regime consists of extinctions and some recolonizations prior to the final extinction of the metapopulation. A summary of the timescales for the different processes and regimes considered in this work can be found in Tables I and II.

A. Competition-dominated dynamics

When $\psi \gg 1$ with $mK < 1$ [slow migration; see Eq. (12)], the carrying capacity is large enough for many migrations to occur on the timescale τ_E of deme extinction, with intrademe dynamics occurring faster than interdeme dynamics. Since every deme expects many incoming cells in time τ_E, deme extinction is unlikely and can be neglected. In this regime, the dynamics is dominated by local M/W competition: W and M cells compete in each deme to fixate the local subpopulation [see Fig. 1(b)].

As in Refs. [41,42,51], the slow migration condition allows us to adopt a coarse-grained description treating each deme as a single entity of type W or M. This is because in the regime of slow migration, the mean time for an M or W invader to fixate a deme is much shorter compared to $1/(mK)$, the expected time between migrations [see Appendix C, Table I, and Eq. (12)]. When the dynamics is dominated by W/M competition and $mK < 1$, at a coarse-grained level, each deme can thus be regarded as being either entirely occupied by W

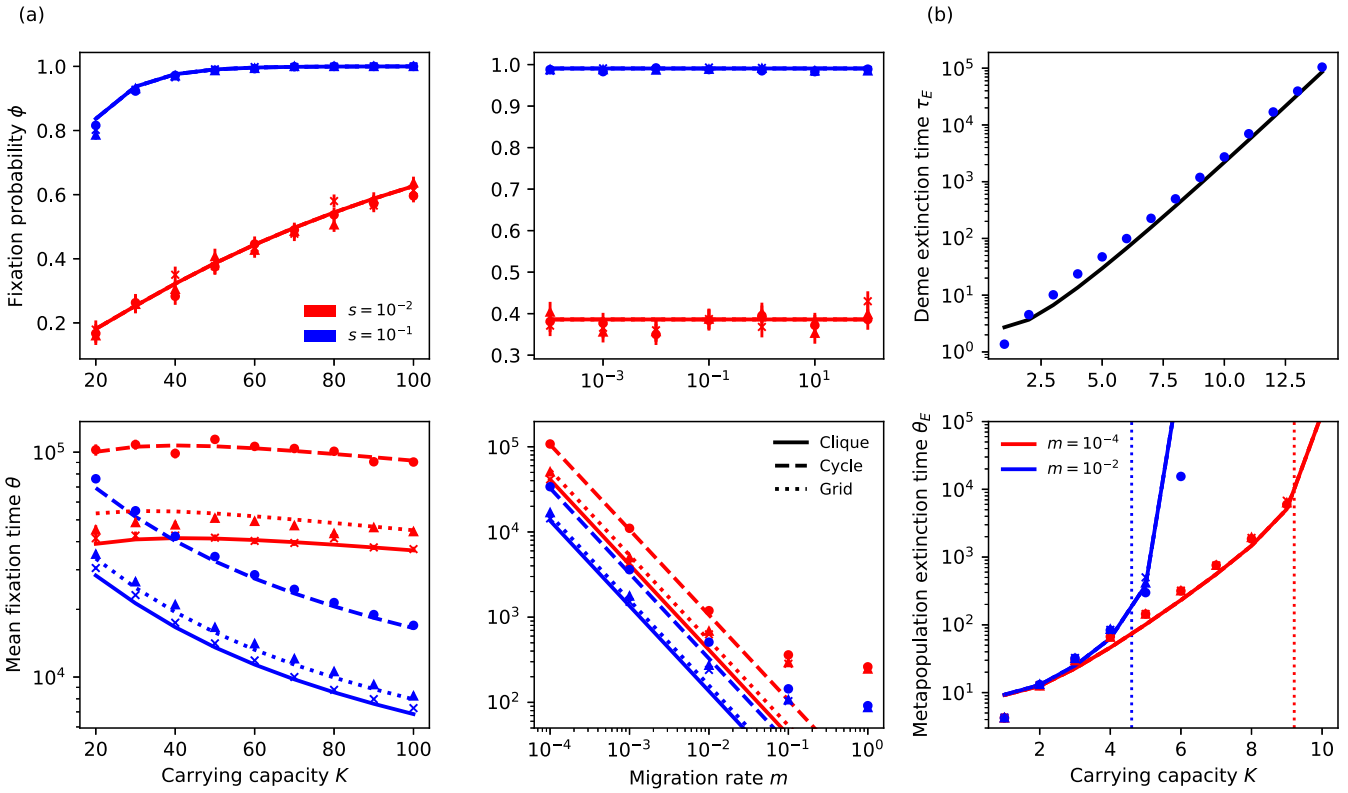

FIG. 2. (a) Competition-dominated dynamics, $\psi \gg 1$. Top left: M fixation probability ϕ vs constant carrying capacity K. Bottom left: Unconditional mean fixation time θ vs K. Top right: ϕ vs per capita migration rate m. Bottom right: θ vs m. Markers are simulation results and lines are predictions of Eq. (14) for $s = 0.1$ (blue) and $s = 0.01$ (red) on a clique (solid lines/crosses), cycle (dashed lines/circles), and grid (dotted lines/triangles). In left, $m = 10^{-4}$ and $\Omega = 16$, and in right, $K = 50$ and $\Omega = 16$. On top, markers for the same s are almost indistinguishable indicating independence of the spatial structure. (b) Extinction-dominated dynamics, $\psi < 1$. Top: Mean extinction time of a single deme τ_E vs K ($m = 0$). Circles are simulation data, line shows the predictions of Eq. (7). Bottom: Metapopulation mean extinction time θ_E vs K for $\Omega = 16$ and $m = 10^{-2}$ (blue) and 10^{-4} (red). Markers are simulation results and thick lines are predictions of Eq. (C4) for cliques (solid lines/crosses), cycles (dashed lines/circles), and grids (dotted lines/triangles). Thin dashed vertical lines are guides to the eye showing $\psi = 1$ for $m = 10^{-2}$ (blue) and 10^{-4} (red). Selection plays no role in this regime, so simulation data for panel (b) have been obtained with $s = 0$. In all panels, there is initially one M deme and $\Omega - 1$ demes occupied by W. In panels (a, top) and (b, bottom), dashed lines overlap with solid lines and so are not visible. Error bars are plotted in each case but are typically too small to see.

or M individuals [see Figs. 1(c) and 1(e)]. In this regime, each sequential migration is an invasion attempt, with a cell from an M/W site trying to invade a neighboring W/M deme [see Fig. 1(c)]. Here, an M/W invasion is the fixation of a single M/W mutant in a deme consisting of $K - 1$ cells of type W/M.

In the realm of the coarse-grained description, the state of the metapopulation in this regime is denoted by i, where $i = 0, 1, \ldots, \Omega$ is the number of demes of type M leaving $\Omega - i$ demes of type W. The probability $\rho_{M/W}$ of invasion by an M/W migrant is here given by the probability that a single M/W cell takes over a population of constant size K in a Moran process [7,64–67] and, as shown in Appendix B, reads

$$\rho_M(K) = \frac{1}{1+s}\left[\frac{s}{1-(1+s)^{-K}}\right],$$
$$\rho_W(K) = \frac{1}{(1+s)^K}\left[\frac{s}{1-(1+s)^{-K}}\right]. \qquad (10)$$

In each time unit, a deme receives from and sends to its neighbors an average of mK cells. Importantly, only edges connecting M and W demes can lead to invasions [see Fig. 1(c)]. These are "active edges" and their number in state i on graph G is denoted by $E_{\mathrm{G}}(i)$, where we consider $\mathrm{G} = \{\text{clique, cycle, grid}\}$. Moreover, migration from a deme can occur to any of the q_{G} neighbors of the deme, where $q_{\text{clique}} = \Omega - 1$, $q_{\text{cycle}} = 2$, $q_{\text{grid}} = 4$, and $q_{\text{d-dim}} = 2d$ for a d-dimensional regular lattice. The number of active edges generally varies with the metapopulation state and the spatial structure, and is difficult to determine. However, a clique being the fully connected graph, the i demes of type M are connected to the $\Omega - i$ demes of type W, yielding $E_{\text{clique}}(i) = i(\Omega - i)$. The M demes of a clique form a single unbreakable cluster since all demes are connected. For a cycle, if the initial state is $i = 1$, the M deme is initially connected to exactly two W demes. This property is conserved by the coarse-grained dynamics on a cycle, with an unbreakable cluster of M demes always connected to a cluster of W demes by two active edges until W or M fixes the metapopulation, yielding $E_{\text{cycle}}(i) = 2$ for $i \neq 0, \Omega$ [see Figs. 1(a) and 1(c) and below].

TABLE I. Typical timescales in metapopulation dynamics.

Process	Timescale for	Expression
Deme size growth	Time for deme size to reach equilibrium	$\sim \ln K = \mathcal{O}(1)$
Deme fixation	Time for fixation in single deme	$\sim 1/s$ [7,66,67]
Migration	Expected time between migration events	$\frac{1}{mK}$
Deme extinction	Mean extinction time of isolated deme	$\tau_E(K) \approx \frac{e^K}{K}$
Metapopulation extinction	Extinction time for full metapopulation	$\theta_E \approx \tau_E \ln \Omega$
Metapopulation fixation	Unconditional mean fixation time	Unwieldy expression
Environmental switching	Correlation time of the dichotomous Markov noise	$\frac{1}{2\nu}$

The unbreakable nature of the M cluster in these two cases (and the symmetric nature of the graphs), means there is only one possible metapopulation state for a given size of M cluster. This allows us to obtain the above explicit expressions for $E_{\text{clique,cycle}}(i)$.

The number of active edges in a grid is difficult to find because the cluster of demes is not unbreakable on a two-dimensional lattice, and there are many possible metapopulation states for a given number of M demes. However, in Appendix E, we show that the average number of active edges on a grid, starting from the metapopulation state $(i, \Omega - i) = (1, \Omega - 1)$, can be approximated by $2\sqrt{\pi i}$. We will, therefore, approximate $E_{\text{grid}}(i) \approx 2\sqrt{\pi i}$ for $i \neq 0, \Omega$. When $i = 0, \Omega$, one strain fixates the entire metapopulation, where all demes are M if $i = \Omega$ and all demes are W when $i = 0$, and hence $E_{\text{G}}(0) = E_{\text{G}}(\Omega) = 0$.

In the coarse-grained description of the competition-dominated dynamics, starting from a single M deme ($i = 1$), there are $mKE_{\text{G}}(i)/q_{\text{G}}$ expected migration attempts per unit time to grow the number of M demes by invading neighboring W demes. Since the probability of an M invasion is ρ_M, given by Eq. (10), the number of M demes grows at a rate $mKE_{\text{G}}(i)\rho_M/q_{\text{G}}$. Similarly a W invader attempts to increase the number of W demes by invading M demes, hence reducing the number of M demes, at a rate $mKE_{\text{G}}(i)\rho_W/q_{\text{G}}$. In this representation, M and W invasions therefore act at the interface of M and W demes by increasing or reducing the number i of M demes at respective rates [41,42,60],

$$T_i^+(m, \text{G}, K) = mK\frac{E_{\text{G}}(i)}{q_{\text{G}}}\rho_M,$$
$$T_i^-(m, \text{G}, K) = mK\frac{E_{\text{G}}(i)}{q_{\text{G}}}\rho_W. \tag{11}$$

These rates, together with the fact that the timescale of intrademe dynamics is $1/s$ (timescale of fixation of a single isolated deme [7,64–67]; see Table I) can be used to define slow migration in the competition-dominated regime. To this end, we notice that the growth of the cluster of i mutant demes in time $1/s$ is $T_i^+(m, \text{G}, K)/s = mKE_{\text{G}}(i)\rho_M/(q_{\text{G}}s)$ [68]. In the coarse-grained description, slow migration is the regime where invasion can be regarded as being instantaneous, with fixation of a successful M invader occurring before the next invasion. This requires that the average number of successful M invasions on the timescale of the intrademe dynamics is less than 1, i.e., $T_i^+(m, \text{G}, K)/s < 1$. Therefore, the condition for slow migration here is

$$m < \frac{sq_{\text{G}}}{K\rho_M E_{\text{G}}(i)} \leqslant \frac{s}{K\rho_M}, \tag{12}$$

where we have used $q_{\text{G}}/E_{\text{G}}(i) \leqslant 1$. When $s \ll 1$ and $Ks \gg 1$, we have $\rho_M \sim s$ [7,64–67] and there is slow migration when $mK \lesssim 1$, i.e., the expected number of migrants from a deme per unit time is less than 1. For typical values used here, e.g., $\Omega = 16$, $K = 100$, and $s = 0.1$, we estimate that there is

TABLE II. Dynamical regimes and their characteristics.

Regime	Condition	Characteristics	Dependence
		Static environment	
Competition-dominated	$\psi \gg 1$	Mutant and wild-type species compete for demes until fixation of the metapopulation	ϕ independent of m and G
Extinction-dominated	$\psi < 1$	Rapid metapopulation extinction	θ_E independent of G
Intermediate	$\psi \gtrsim 1$	Competition between demes with stochastic deme extinction and recolonization. Fraction of occupied demes: $\frac{\Omega_{\text{occ}}}{\Omega} \approx 1 - \frac{1}{\psi}$	Weak G dependence of ϕ_{int} (See Eq. (F3) and Appendix F)
		Time-varying environment	
Weak bottlenecks	$\psi(m, K_-) \gg 1$	Nonmonotonic ν-dependence of Φ^{G}, Θ^{G}	Φ^{G} depends on m
Strong bottlenecks	$\psi(m, K_-) < 1$	Extinction possible at ν extremes. Mutant removal optimal at intermediate ν	Independent of G

slow migration if $m \lesssim 10^{-2}$, which is in line with the values of $m \in [10^{-5}, 10^{-2}]$ used in our examples, and explains the deviations reported in Fig. 2(a) (bottom right) for larger m. The coarse-grained competition-dominated dynamics is thus a birth-death process for the number i of M demes, with absorbing boundaries at $i = \Omega$ (M fixation) and $i = 0$ (W fixation) (see Appendix G). In this representation, the M fixation probability in a metapopulation of size Ω, spatially structured as a graph G, consisting initially of i mutant demes is denoted ϕ_i^{G}, and the unconditional (i.e., regardless of whether M or W takes over [7,66,67]) mean fixation time (uMFT) denoted θ_i^{G}. These quantities satisfy the first-step equations [7,66,67,73]

$$\begin{aligned}(T_i^+ + T_i^-)\phi_i^{\mathrm{G}} &= T_i^+\phi_{i+1}^{\mathrm{G}} + T_i^-\phi_{i-1}^{\mathrm{G}},\\ (T_i^+ + T_i^-)\theta_i^{\mathrm{G}} &= 1 + T_i^+\theta_{i+1}^{\mathrm{G}} + T_i^-\theta_{i-1}^{\mathrm{G}},\end{aligned} \tag{13}$$

for $i = 1, \ldots, \Omega - 1$, with boundary conditions $\phi_0^{\mathrm{G}} = 1 - \phi_\Omega^{\mathrm{G}} = 0$ and $\theta_0^{\mathrm{G}} = \theta_\Omega^{\mathrm{G}} = 0$. The recurrence relations (13) can be solved exactly [66,67] (see also Appendix B). Here, we are chiefly interested in the fixation of a single initial M deme, $i = 1$, and simply write $\phi^{\mathrm{G}} \equiv \phi_1^{\mathrm{G}}$ and $\theta^{\mathrm{G}} \equiv \theta_1^{\mathrm{G}}$, finding

$$\begin{aligned}\phi^{\mathrm{G}}(K) &= \phi(K) = \frac{1-\gamma}{1-\gamma^\Omega},\\ \theta^{\mathrm{G}}(m,K) &= \frac{1-\gamma}{1-\gamma^\Omega}\sum_{k=1}^{\Omega-1}\sum_{n=1}^{k}\frac{\gamma^{k-n}}{T_n^+(m,\mathrm{G},K)},\end{aligned} \tag{14}$$

where $\gamma \equiv T_i^-/T_i^+ = \rho_W/\rho_M \approx \exp(-Ks)$ is a quantity independent of m and G. As noted in Refs. [41,42,50], the fixation probability $\phi^{\mathrm{G}} = \phi$ is therefore independent of the migration rate and spatial structure. This remarkable result stems from the graphs considered here being circulations [see Eq. (5)]. In *static environments*, a generalized circulation theorem ensures that the fixation probability is independent of m and G for circulation graphs [41,42,47], a feature displayed in the stochastic simulations of Fig. 2(a) (top) for the full microscopic model. In excellent agreement with simulation data of Fig. 2(a) (top), we find that the M fixation probability increases almost exponentially with Ks and approaches 1 when $Ks \gg 1$, $\phi^{\mathrm{G}} \approx 1$. This stems from the invasion of W demes being increasingly likely (and the invasion of M demes exponentially less likely) when the average number of migrations (mK) increases along with K. When $Ks \ll 1$, the competition is effectively neutral, and in this case, $\phi^{\mathrm{G}} \approx 1/\Omega$. In good agreement with simulation results of Fig. 2(a) (bottom), Eq. (14) predicts that the uMFT decreases with the migration rate $\theta^{\mathrm{G}} \sim 1/m$ and, for given parameters, the uMFT is shortest on cliques, while it is larger on cycles than on grids. Intuitively, for higher m and more connected graphs, migrants spread faster leading to quicker invasion and fixation.

B. Extinction-dominated dynamics

In the extinction-dominated regime $\psi < 1$ with $mK < 1$ (slow migration), we do not expect any deme invasions in a time τ_E, enabling us to adopt a suitable coarse-grained description. Deme invasions being negligible under slow migration, the timescale of extinction dynamics is much shorter than that of M/W competition, and site extinction dominates over deme invasion [see Fig. 1(e)]. The dynamics in this extinction-dominated regime is hence governed by the random extinction of demes, regardless of their type. Following Ref. [59], in the realm of the coarse-grained description outlined in Appendix C, demes are regarded as being either occupied (by either W or M cells) or empty. Deme extinction occurs randomly while empty demes may be recolonized by migrations from occupied neighboring demes, which occur rarely in this regime. Since spatial structure may only influence the dynamics via migrations, the coarse-grained dynamics is largely independent of the spatial structure in this regime where $mK < 1$, and can be represented by a birth-death process for the number of occupied demes, assuming that the site extinction and recolonization occur instantaneously [59] (see Appendix C). In this coarse-grained representation, when all demes are initially occupied ($n = K$), the metapopulation mean extinction time (mMET), denoted by θ_E, is given by Eq. (C4) in Appendix C. When $\Omega \gg 1$ and $\psi < 1$, the leading contribution to the mMET arises from the term $i = n$ in the innermost sum, yielding

$$\theta_E(K,\Omega) \approx \tau_E(\ln(\Omega) + \gamma_{\mathrm{EM}}), \tag{15}$$

where $\gamma_{\mathrm{EM}} \approx 0.577...$ is the Euler-Mascheroni constant. Equation (15) gives a good approximation of the mMET as reported in Fig. 8. As ψ increases with K, at the upper limit of the extinction-dominated limit (where ψ approaches 1), the mMET grows almost exponentially with K and logarithmically with Ω, $\theta_E \approx e^K \ln(\Omega)/K$. Equation (C4) thus predicts a rapid growth of the mMET when $\psi \gtrsim 1$, as shown in Fig. 2(b) (bottom), where simulation results are found to be in good agreement with Eq. (C4).

When $\psi \gtrsim 1$, the competition- and extinction-dominated dynamics are separated by an intermediate crossover regime analyzed in detail in Appendix F.

IV. TIME-FLUCTUATING ENVIRONMENTS

Microbial populations generally evolve in time-varying environments, and are often subject to conditions changing suddenly and drastically, e.g., experiencing cycles of harsh and mild environmental states [20,25,28,30,74–84] (see Fig. 3). These variations cause fluctuations often associated with population *bottlenecks*, arising when the deme size is drastically reduced, e.g., due to nutrient scarcity or exposure to toxins [25,27–29,31]. Here, environmental variability is encoded in the time-fluctuating carrying capacity $K(t)$ of Eq. (6) driven by the DMN $\xi(t) \in \{-1, 1\}$ [16–24,32,69–71] (see Sec. II). Since the dynamics of the deme size n occurs on a timescale of order 1 (see Appendix A 2), the variable n tracks $K(t)$ and experiences a bottleneck whenever the carrying capacity switches from K_+ to K_- at a rate $\nu \lesssim 1$ [see Fig. 3(a), right] [16–18].

In order to study the joint effect of migration and fluctuations on the metapopulation dynamics, we assume $K_+ \gg 1$ such that demographic fluctuations are weak in the mild environment. In what follows, we distinguish between weak bottlenecks, where $\psi(m, K_-) \gg 1$ and deme extinction is negligible, and strong bottlenecks, where $\psi(m, K_-) < 1$ and deme extinctions dominate.

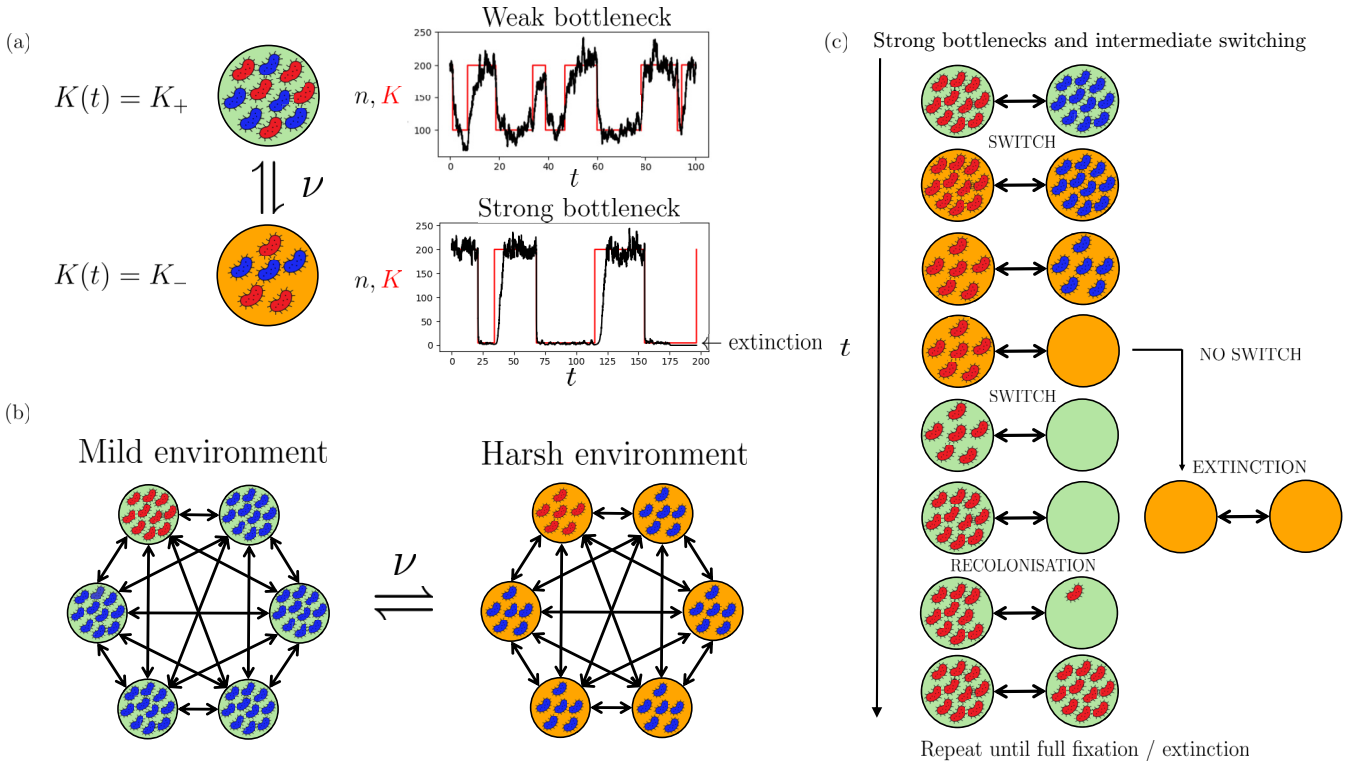

FIG. 3. (a) Left: Single deme in time-switching environment. The carrying capacity $K(t)$ encodes environmental variability by switching between $K = K_+$ (mild environment, green/light) and $K(t) = K_- < K_+$ (harsh environment, orange/dark) at symmetric rate ν (see also Appendix H). Communities are larger in the mild environment. When $K(t)$ switches at an intermediate rate $\nu \lesssim 1$, each deme experiences bottlenecks prior to deme fixation at an average frequency $\nu/2$ (see text). Right: n and K vs time in the intermediate switching regime where the size n of a deme undergoes bottlenecks. Parameters are $K_+ = 200$, $\nu = 0.05$, and $K_- = 100$ (top) and $K_- = 5$ (bottom). The bottlenecks are weak when $\psi(m, K_-) \gg 1$ (top, right) where deme extinction is unlikely. When $\psi(m, K_-) < 1$, there are strong bottlenecks and each deme can go extinct in the harsh environment (bottom, right). (b) Clique metapopulation with $\Omega = 6$ connected demes (double arrows). All demes have the same time-switching carrying capacity $K(t)$ encoding environmental variability across the metapopulation, with each deme in the same environmental state. (c) Example evolution across two nearest-neighbor demes in a switching environment subject to strong bottlenecks in the intermediate switching regime (see text). Starting in the mild environment where $K = K_+$, the carrying capacity switches to K_- (harsh environment) after $t \sim 1/\nu$. Following the $K_+ \to K_-$ switch, each deme size decreases and each subpopulation is subject to strong demographic fluctuations and hence prone to extinction. In the absence of recolonization of empty demes, effective only in the mild state, all demes go extinct. If there is a switch back to the mild environment $K_- \to K_+$ prior to total extinction, empty demes can be rescued by migration and recolonized by incoming W or M cells from neighboring demes. In the sketch, an empty deme is recolonized by a mutant in the mild environment and becomes an M deme. The cycle continues until the entire metapopulation consists of only W or M demes, or metapopulation extinction.

A. Weak bottlenecks: $\psi(m, K_-) \gg 1$

When $K_+ > K_-$ with $\psi(m, K_-) \gg 1$, each deme experiences a weak bottleneck at an average frequency $\nu/2$ when $\nu \lesssim 1$ [16–18] [see Fig. 3(a), top]. The condition $\psi(m, K_-) \approx me^{K_-} \gg 1$ ensures that deme extinction can be neglected, with metapopulation dynamics dominated by M/W competition. The metapopulation fate can thus be captured by a two-state coarse-grained description similar to that of Sec. III A. Since the deme size in the environment ξ, and thus the number of migrating cells, varies with $K(t)$, it is useful to introduce the long-time average deme size in environmental state $\xi = \pm 1$ under switching rate ν denoted by $\mathcal{N}_\xi(\nu) \equiv \mathcal{N}_\pm(\nu)$; see below.

We first discuss the metapopulation fate in the limit of slow and fast environmental switching, and then return to the above case of weak bottlenecks with $\nu \lesssim 1$.

When the environment varies very slowly, $\nu \ll 1$, the carrying capacity remains at its initial value, i.e., $K(t) = K_+$ or $K(t) = K_-$ each with a probability $1/2$, until invasions lead to the fixation of W or M. In other words, the time between switches is longer than the mean fixation time in each environment such that $\nu \max(\theta^{\mathrm{G}}(m, K_+), \theta^{\mathrm{G}}(m, K_-)) < 1$, where $\theta^{\mathrm{G}}(m, K)$ is given by Eq. (14). In the slow switching regime, the M fixation probability and uMFT on a metapopulation spatially arranged as a regular graph G are, respectively, denoted by Φ_0^{G} and Θ_0^{G}. The quantities are obtained by averaging their static counterparts [Eq. (14)] over the stationary distribution of K, yielding for symmetric switching

$$\Phi_0^{\mathrm{G}}(m, K_\pm) = \Phi_0(K_\pm) = \tfrac{1}{2}[\phi(K_+) + \phi(K_-)],$$
$$\Theta_0^{\mathrm{G}}(m, K_\pm) = \tfrac{1}{2}[\theta^{\mathrm{G}}(m, K_+) + \theta^{\mathrm{G}}(m, K_-)]. \qquad (16)$$

When the environment varies very quickly, $\nu \gg 1$, the DMN self-averages before invasion-mediated fixation occurs, and the carrying capacity of each deme rapidly reaches the

effective value

$$\mathcal{K} \equiv \frac{2K_+K_-}{K_+ + K_-}, \tag{17}$$

the harmonic mean of K_+ and K_-, with $\mathcal{K} \approx 2K_-$ if $K_- \gg 1$, and $\mathcal{N}_\pm(\infty) \to \mathcal{K}$ when $\mathcal{K} \gg 1$ [16–18,22] (see Appendix A 2). In this fast switching regime, the M fixation probability and uMFT on a metapopulation spatially arranged as a regular graph G, respectively, denoted by $\Phi^{\rm G}_\infty$ and $\Theta^{\rm G}_\infty$, are obtained by replacing K with $\mathcal{K}$ in Eq. (14), yielding

$$\begin{aligned}\Phi^{\rm G}_\infty(m,\mathcal{K}) &= \Phi_\infty(\mathcal{K}) = \phi(\mathcal{K}),\\ \Theta^{\rm G}_\infty(m,K_\pm) &= \theta^{\rm G}(m,\mathcal{K}).\end{aligned} \tag{18}$$

From these expressions and Eq. (14), we notice that the fixation probability in the regime of slow and fast switching is independent of the migration rate and spatial structure: $\Phi^{\rm G}_0 = \Phi_0$ and $\Phi^{\rm G}_\infty = \Phi_\infty$. However, the metapopulation uMFT depends explicitly on the migration rate m and G, with $\Theta^{\rm G}_0 \sim 1/m$ and $\Theta^{\rm G}_\infty \sim 1/m$.

Under intermediate switching rate, when $\nu \lesssim 1$, the coupling of demographic and environmental fluctuations plays a key role, while cell migration depends on the deme size that in turn varies with the environmental state. Here, the metapopulation dynamics cannot be directly related to its static counterpart. The average deme size $\mathcal{N}_\xi(\nu)$ depends nontrivially on ν and ξ, and generally needs to be computed by sampling long-time simulations. However, analytical progress can be made by approximating the distribution of the size n of an isolated deme in the environmental state ξ by the joint probability density $p_\xi(n;\nu)$ of the piecewise deterministic Markov process (PDMP), where n and ξ are variables, and ν a parameter, obtained by ignoring demographic fluctuations [16,17,85,86] (see Appendix A 2):

$$p_\xi(n;\nu) = \begin{cases} \frac{\mathcal{Z}_+}{n^2}\left(\frac{K_+-n}{n}\right)^{\nu-1}\left(\frac{n-K_-}{n}\right)^{\nu} & \text{if } \xi=+1,\\ \frac{\mathcal{Z}_-}{n^2}\left(\frac{K_+-n}{n}\right)^{\nu}\left(\frac{n-K_-}{n}\right)^{\nu-1} & \text{if } \xi=-1.\end{cases} \tag{19}$$

The density $p_\xi(n;\nu)$ has support $[K_-,K_+]$, and the normalization constants $\mathcal{Z}_\pm$ ensure $\int_{K_-}^{K_+} p_\xi(n;\nu)\,{\rm d}n = 1$. The M/W competition characterizing the intermediate switching regime dynamics can be described by the coarse-grained representation of Sec. III A generalized to a time-fluctuating environment following Refs. [16,17,22]. Here, we analyze the influence of ν and m on the M fixation probability, $\Phi^{\rm G}_i(\nu,m)$, and uMFT, $\Theta^{\rm G}_i(\nu,m)$, in a metapopulation consisting of i mutants demes and $\Omega - i$ W demes spatially arranged as a regular graph G. To this end, we consider a birth-death process for the number $i = 0,\ldots,\Omega$ of M demes. As in Sec. III A, we assume that there is initially a single M deme ($i = 1$). The effective rates, denoted by $\mathcal{T}^\pm_{i,\xi}$, for the increase or decrease by one of the number i of M demes in the environmental state ξ depend on the expected number of migrating cells, which in turn depends on the deme size that is now a time-fluctuating quantity driven by Eq. (6). In a time-varying environment, the expected number of migrants from a deme, mn, is approximated by $m\mathcal{N}_\xi(\nu)$, where the long-time mean deme size in the environmental state ξ is obtained from the PDMP density according to

$$\mathcal{N}_\xi(\nu) = \int_{K_-}^{K_+} n p_\xi(n;\nu/s)\,{\rm d}n, \tag{20}$$

where, as in Refs. [16–19,23], the switching rate has been rescaled, $\nu \to \nu/s$, by the timescale of the deme fixation dynamics (see Appendix A 2) where there are an average of $\mathcal{O}(\nu/s)$ switches on the deme fixation timescale [17,18]. The (marginal) average deme size regardless of ξ is given by $\mathcal{N}(\nu) = \frac{1}{2}\sum_\xi \mathcal{N}_\xi(\nu)$ and known to be a decreasing function of ν [16,17]. As in static environments [see Eq. (11)] the transition rates $\mathcal{T}^\pm_i$ depend on the spatial structure, via $E_{\rm G}(i)/q_{\rm G}$, and on the probability $\rho_{M/W,\xi}(\nu)$ that an M/W migrant invades a W/M deme in the environment ξ. Putting everything together, this yields the effective transition rates

$$\begin{aligned}\mathcal{T}^+_{i,\xi}(\nu,m,{\rm G}) &= m\mathcal{N}_\xi(\nu)\frac{E_{\rm G}(i)}{q_{\rm G}}\rho_{M,\xi}(\nu),\\ \mathcal{T}^-_{i,\xi}(\nu,m,{\rm G}) &= m\mathcal{N}_\xi(\nu)\frac{E_{\rm G}(i)}{q_{\rm G}}\rho_{W,\xi}(\nu),\end{aligned} \tag{21}$$

where, by analogy with Eq. (10), we have introduced

$$\begin{aligned}\rho_{M,\xi}(\nu) &\equiv \frac{s}{1+s}\frac{1}{1-(1+s)^{-\mathcal{N}_\xi(\nu)}},\\ \rho_{W,\xi}(\nu) &\equiv \frac{s}{(1+s)^{\mathcal{N}_\xi(\nu)}}\frac{1}{1-(1+s)^{-\mathcal{N}_\xi(\nu)}}.\end{aligned} \tag{22}$$

With Eq. (21), by dropping all explicit dependence except on i and ξ, we obtain the M fixation probability starting from the environmental state ξ with i mutant demes on a graph G, denoted by $\Phi^{\rm G}_{i,\xi}(\nu,m)$, as the solution of the ν-dependent first-step analysis equation

$$[\mathcal{T}^+_{i,\xi} + \mathcal{T}^-_{i,\xi} + \nu]\Phi^{\rm G}_{i,\xi} = \mathcal{T}^+_{i,\xi}\Phi^{\rm G}_{i+1,\xi} + \mathcal{T}^-_{i,\xi}\Phi^{\rm G}_{i-1,\xi} + \nu\Phi^{\rm G}_{i,-\xi}, \tag{23}$$

subject to the boundary conditions $\Phi^{\rm G}_{0,\xi} = 0$ and $\Phi^{\rm G}_{\Omega,\xi} = 1$. The metapopulation uMFT starting from the same initial conditions, denoted by $\Theta^{\rm G}_{i,\xi}$, similarly satisfies

$$[\mathcal{T}^+_{i,\xi} + \mathcal{T}^-_{i,\xi} + \nu]\Theta^{\rm G}_{i,\xi} = 1 + \mathcal{T}^+_{i,\xi}\Theta^{\rm G}_{i+1,\xi} + \mathcal{T}^-_{i,\xi}\Theta^{\rm G}_{i-1,\xi} + \nu\Theta^{\rm G}_{i,-\xi}, \tag{24}$$

with boundary conditions $\Theta^{\rm G}_{0,\xi} = \Theta^{\rm G}_{\Omega,\xi} = 0$. Equations (23) and (24) generalize Eqs. (13) to a time-switching environment, with the last terms on the right-hand side (RHS) accounting for environmental switching, and coupling $\Phi^{\rm G}_{i,\xi}$ to $\Phi^{\rm G}_{i,-\xi}$ and $\Theta^{\rm G}_{i,\xi}$ to $\Theta^{\rm G}_{i,-\xi}$. Equations (23) and (24) can be solved numerically using standard methods. The M fixation probability $\Phi^{\rm G}_i(\nu)$ and uMFT $\Theta^{\rm G}_i(\nu)$ regardless of ξ are obtained by averaging over the stationary distribution of ξ, yielding

$$\begin{aligned}\Phi^{\rm G}_i(\nu,m) &= \frac{1}{2}\sum_\xi \Phi^{\rm G}_{i,\xi}(\nu,m),\\ \Theta^{\rm G}_i(\nu,m) &= \frac{1}{2}\sum_\xi \Theta^{\rm G}_{i,\xi}(\nu,m),\end{aligned} \tag{25}$$

where we have reinstated the explicit dependence on ν and m. As we specifically consider the initial condition of a single M deme, we set $i = 1$ in Eq. (25) and simplify the notation by

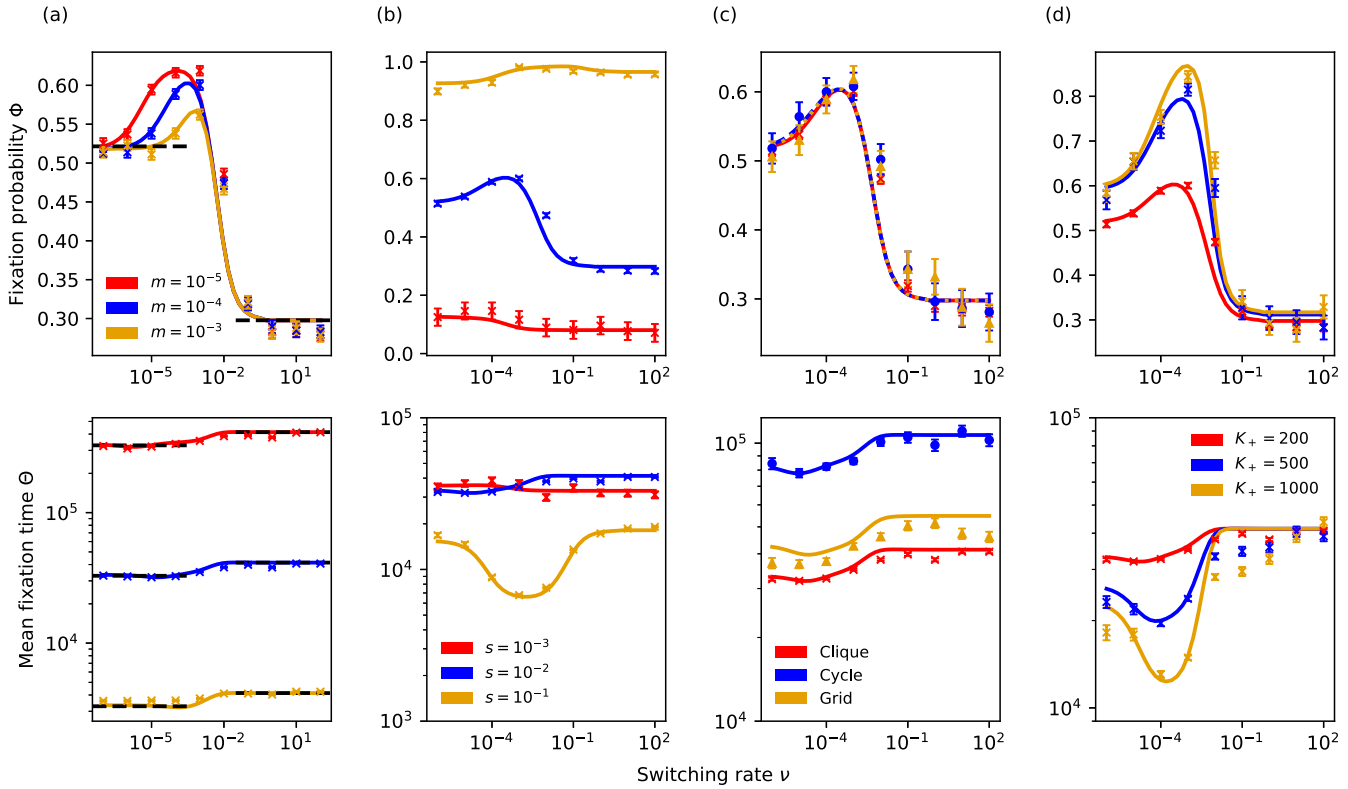

FIG. 4. Fixation probability Φ^{G} and mean fixation time Θ^{G} against switching rate ν for various parameters. Each panel shows Φ^{G} vs ν (top) and Θ^{G} vs ν (bottom). Markers show simulation results and lines are predictions of Eq. (26). $\Phi^{\mathrm{clique}}(\nu)$ and $\Theta^{\mathrm{clique}}(\nu)$ for a clique metapopulation and different values of m in panel (a) and s in panel (b). (a) $m = 10^{-5}$ (red), $m = 10^{-4}$ (blue), $m = 10^{-3}$ (yellow), and $s = 0.01$. (b) $s = 10^{-3}$ (red), $s = 10^{-2}$ (blue), $s = 10^{-1}$ (yellow), and $m = 10^{-4}$. Dashed black lines are guides to the eye showing $\Phi_{0,\infty}$ in panel (a, top) and $\Theta_{0,\infty}$ in (a, bottom) (see text). Other parameters are $\Omega = 16$, $K_+ = 200$, and $K_- = 20$. (c) $\Phi^{\mathrm{G}}(\nu)$ and $\Theta^{\mathrm{G}}(\nu)$ for clique (red, crosses), cycle (blue, circles), and grid (yellow, triangles) metapopulations. Other parameters are $\Omega = 16$, $K_+ = 200$, $K_- = 20$, $s = 0.01$, and $m = 10^{-4}$. (d) $\Phi^{\mathrm{clique}}(\nu)$ and $\Theta^{\mathrm{clique}}(\nu)$ for a clique metapopulation with $K_+ = 200$ (red), $K_+ = 500$ (blue), and $K_+ = 1000$ (yellow). Deviations occur for Θ with $K_+ = 1000$ since the slow-migration condition is not satisfied in the mild environment. Other parameters are $\Omega = 16$, $K_- = 20$, $s = 0.01$, and $m = 10^{-4}$. In all examples, there is initially a single M deme and $\Omega - 1$ others of type W (see text).

writing

$$\Phi^{\mathrm{G}}(\nu, m) = \Phi_1^{\mathrm{G}}(\nu, m) \quad \text{and} \quad \Theta^{\mathrm{G}}(\nu, m) = \Theta_1^{\mathrm{G}}(\nu, m). \quad (26)$$

Equation (26) are the expressions of the M fixation probability and metapopulation uMFT in the realm of the combined coarse-grained and PDMP description. This approach is valid under slow migration rate ($mK < 1$) and weak selection strength ($s \ll 1$) for the assumption $n \approx \mathcal{N}_{\xi}(\nu)$ to hold at each invasion (see Appendix A 2). In Fig. 4, the comparison of the predictions of Eq. (26) with the simulation results of the full model on the regular graphs G = {clique, cycle, grid} shows that Eq. (26) captures well the dependence of Φ^{G} and Θ^{G} on ν, m, s, and K_+. In particular, Eq. (26) reproduces on all G the nonmonotonic ν dependence of Φ^{G} and Θ^{G} (when it exhibits this feature), as well as their behavior when $\nu \to 0, \infty$ given by Eqs. (16) and (18).

A striking feature of Φ^{G} and Θ^{G} is their dependence on spatial migration. In Fig. 4(a) (top), we indeed find that simulation data for $\Phi^{\mathrm{clique}}(\nu, m)$ vary noticeably with m in the range $\nu \in [10^{-4}, 10^{-1}]$. These deviations, of up to 20%, exceed the error bars and are reasonably well captured by Eq. (26). In Fig. 4(c) (top), we notice that both simulation results and predictions of Eq. (26) for $\Phi^{\mathrm{G}}(\nu, m)$ differ slightly for each graph G, whereas Fig. 4(c) (bottom) shows that Θ^{G} clearly depends on the spatial structure. The explicit dependence of the fixation probability on migration and spatial structure is in stark contrast with the result Eq. (14) obtained in static environments, and is therefore a signature of the ecoevolutionary dynamics in time-fluctuating environments. As shown in Appendix G, the correspondence demonstrated in Ref. [41] between Φ^{G} and the fixation probability of a random walk for the number $i = 0, 1, \ldots, \Omega$ of mutant demes with hopping probabilities independent of m and G, and absorbing states 0, Ω, breaks down in time-varying environments. This leads to the dependence of Φ^{G} and Θ^{G} on m and G in time-switching environments.

Another distinctive feature of Φ^{G} and Θ^{G} is their nonmonotonic ν dependence when the other parameters (s, m, $K_{\pm}$, Ω) are kept fixed. In particular, Fig. 4 shows that Φ^{G} may exhibit a sharp peak in the regime of intermediate $\nu \in [10^{-4}, 10^{-1}]$ that is well captured by Eq. (26). These results are in marked contrast with their counterparts in a single deme, which vary monotonically with ν [16,17,19]. The nonmonotonic ν dependence of Φ^{G} and Θ^{G} is therefore an inherent effect of spatial migration. Intuitively, this behavior stems, on the one hand, from more M invasions occurring

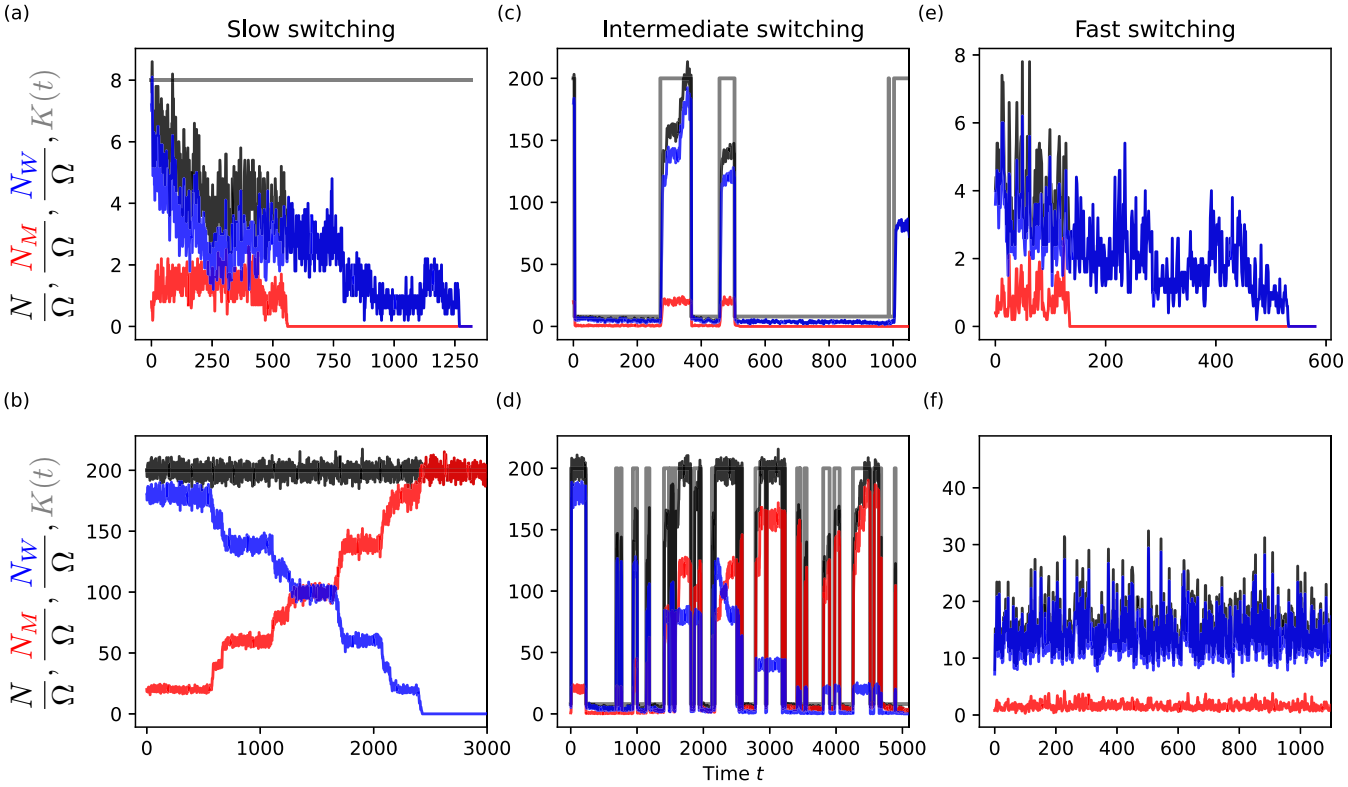

FIG. 5. Typical single realizations of N/Ω (black), N_M/Ω (red), N_W/Ω (blue), and $K(t)$ (gray) against time for different values of K_- and ν. Here, $\nu = 10^{-4}$ and $K_- = 8$. In panel (a), $K = K_-$ at $t = 0$ and M and then W quickly go extinct. In panel (b), $K = K_+$ at $t = 0$ and M fixes the population while W goes extinct. (c), (d) Here, $\nu = 10^{-2}$ and $K_- = 8$. In panel (c), mutants survive the first few bottlenecks but their abundance is low leading to the fixation of W and removal of M after four bottlenecks ($t \gtrsim 1000$). In panel (d), mutants survive the first bottlenecks and spread in the mild state where they recolonize and invade demes. They are eventually able to fix the population. Here, $\nu = 10$, and $K_- = 4$ in panel (e) and $K_- = 10$ in panel (f). $K(t)$ switches very frequently and is not shown for clarity. In panel (e), the deme size is $n \approx 2K_- = 8$ and the dynamics is dominated by deme extinction leading to the rapid extinction of the metapopulation. In panel (f), the deme size is $n \approx 2K_- = 20$ and there is M/W competition that leads to fixation of M and extinction of W after a typical time $t \sim \theta^{\text{clique}}(2K_-) \gtrsim 10^4$ (not shown). Similar results are obtained on other regular graphs G (see text). Other parameters are $\Omega = 10$, $s = 0.1$, $m = 10^{-4}$, and $K_+ = 200$. In all panels, initially there is a single M deme and $\Omega - 1$ demes occupied by W.

when the deme size is as close as possible to $n \approx K_+$ [see Eq. (21)]. On the other hand, the average deme size is a decreasing function of ν [16–18] (see Appendix A 2). Therefore, optimizing the probability of M fixation requires two considerations: The environment should avoid remaining stuck in the harsh environment for too long, which can happen with a probability close to $1/2$ when $\nu \ll 1$, and the environment should not switch too frequently (i.e., $\nu \gg 1$), as this reduces the effective deme size ($n \approx \mathcal{K}$), which can be significantly smaller than K_+. Hence, the best conditions for the fixation of M are for a range of ν in the intermediate regime. Since the uMFT is longer in the harsh than in the mild environment [where there are fewer migration events; see Fig. 2(a), bottom left], a similar reasoning leads to a minimum mean fixation time for ν in the intermediate regime [see Figs. 4(b) and 4(d)].

B. Strong bottlenecks: $\psi(m, K_-) < 1$

When $\psi(m, K_-) < 1$, each deme can undergo strong bottlenecks [see Fig. 3(a) and below]. In the harsh environment $\xi = -1$ ($K = K_-$), the entire metapopulation experiences extinction, in an observable time $\theta_E(K_-, \Omega)$, denoted θ_E here for conciseness. However, in the mild state $\xi = +1$ ($K = K_+$), deme extinction can be neglected and each site can be regarded as being occupied by either W or M cells. The dynamics in the harsh state is thus dominated by extinction, whereas the M/W competition characterizing the mild state is aptly captured by the two-state coarse-grained description of Sec. III A. Environmental switching thus couples regimes that are dominated in turn by deme extinction and M/W competition, yielding complex dynamical scenarios whose analysis is difficult. However, we can gain valuable insight by considering first the limits $\nu \ll 1$, $\nu \gg 1$, and then the case of intermediate switching where $\nu \lesssim 1$.

When the environment varies very slowly, $\nu \ll 1$, the $K(t)$ remains at its initial value for long periods, that is $K = K_\pm$ if $\xi(0) = \pm 1$ each with a probability $1/2$. On the one hand, if initially $\xi = -1$ (harsh environment), $K = K_-$ and each deme is prone to extinction after a mean time $\tau_E(K_-)$, which eventually leads to the collapse of the metapopulation after an mMET $\theta_E \approx e^{K_-} \ln(\Omega)/K_-$ when $\Omega \gg 1$ and $K_- \gg 1$ [see Eqs. (7) and (15) and Fig. 5(a)]. On the other hand, if initially $\xi = +1$ (mild condition), $n \approx K_+$ and there is M/W competition characterized by the fixation of M with a probability $\phi(K_+)$ approaching 1 when $K_+ s \gg 1$ [see Eq. (14)

and Fig. 5(b)]. As a result, when $\nu \ll 1$ and $K_+ s \gg 1$, there are two equally likely outcomes illustrated in Fig. 5: either the extinction of the metapopulation in a mean time θ_E as in Fig. 5(a), or the fixation of M after a mean time $\theta^{\mathrm{G}}(K_+)$ as in Fig. 5(b).

In frequently varying environments, when $\nu \gg 1$, the size of each deme readily settles about the effective carrying capacity Eq. (17), with $n \approx \mathcal{K}$ (when $\mathcal{K} \gg 1$) after $t \sim 1$ [16,17]. Since $\mathcal{K} \approx 2K_-$ when $K_+ \gg K_-$, if $\psi(m, 2K_-) < 1$ the dynamics is characterized by the extinction of individual demes and then of the entire metapopulation after mean times $\tau_E(2K_-)$ and $\theta_E(\Omega, 2K_-)$ [see Fig. 5(e)]. However, if $\psi(m, 2K_-) \gg 1$ and $2K_- s \gg 1$, the dynamics is characterized by M/W competition with M most likely to fix the metapopulation after a mean time $\theta^{\mathrm{G}}(2K_-)$, as illustrated by Fig. 5(f).

In slowly and rapidly changing environments, regardless of the spatial structure, the metapopulation subject to strong bottlenecks is therefore always at risk of either complete extinction or of being taken over by mutants.

In the intermediate switching regime, $\nu \lesssim 1$ with $\psi(m, K_-) < 1$, each deme is subject to strong bottlenecks [16–18] [see Appendix A (and first paragraph of Sec. IV)]. In this regime, the entire metapopulation therefore experiences strong bottlenecks and can avoid extinction for extended periods of time while either strain can prevail. In the harsh environmental state ($K = K_-$), the dynamics is always dominated by deme extinction. In the mild state ($K = K_+ \gg K_-$), there is recolonization of empty demes that rapidly become either W or M demes, followed by invasions and M/W competition. In order to ensure that the collapse of the metapopulation is unlikely to be observed, the mean time spent in either environmental state needs to be shorter than the metapopulation mean extinction time in the harsh environment, i.e., $1/\nu < \theta_E$. Moreover, when $\nu \sim 1/\tau_E(K_-) > 1/\theta_E$, numerous demes go extinct in the harsh environment before switching to the mild state. Hence, when $\nu \lesssim 1$ and $\nu\theta_E > 1$, the metapopulation is unlikely to go extinct and transiently consists of a mixture of empty demes and W/M demes before either W or M eventually takes over. In this regime, mutants are likely to be removed from the metapopulation when there is a small fraction of them in the harsh environment [see Fig. 5(c)]. At each strong bottleneck, M demes have a finite probability to go extinct before switching to the mild environment, where surviving mutants can invade W demes and recolonize empty demes. In a scenario illustrated by Fig. 5(c), there are periods of duration $\sim 1/\nu$ during which the number of mutants remains low and prone to extinction when $K = K_-$, followed by periods in K_+ where the number of M demes increases (due to M/W competition). Each bottleneck can thus be regarded as an attempt to remove M demes, whereas each switch $K_- \to K_+$ can be envisioned as a rescue of mutants. This cycle repeats itself until M demes are entirely removed after enough bottlenecks. The metapopulation thus consists of a fluctuating number of W demes and empty demes. This scenario is the most likely to occur when the initial fraction of M demes is small. Another possible outcome, illustrated by Fig. 5(d), occurs when mutants surviving the harsh conditions invade and are successful in recolonizing many demes in the mild environment. Mutants can thus significantly increase the number of M demes, exceeding that of W demes. In this case, bottlenecks can be seen as an attempt to remove W and M demes, and the most likely outcome is the removal of W demes. In this scenario, the metapopulation eventually consists of a fluctuating number of empty demes and mutant demes, as illustrated by Fig. 5(d). The results of Fig. 5 have been obtained for cliques, but the same qualitative behavior is expected for any regular graphs G, with the spatial structure affecting the long-term fraction of occupied demes and therefore the probability of removal of each bottleneck. However, phenomena operated by extinction are mostly independent of G and m, as illustrated by Fig. 10.

A hypothetical idealized treatment strategy: In this intermediate switching regime, the metapopulation is likely to avoid extinction in the harsh environment if $\nu\theta_E \gtrsim 1$. Moreover, when $mK_+\theta_E \gtrsim 1$, then enough demes are recolonized in the mild environment to ensure that the metapopulation will not readily go extinct after a bottleneck. Hence, the metapopulation is likely to avoid extinction when $\nu\theta_E > 1$ and $mK_+\theta_E > 1$. In this scenario, either W or M can be entirely removed, with respective probabilities Φ and $1 - \Phi$, after a mean time Θ, while metapopulation extinction occurs after a mean time $\Theta_E \gg \Theta$. As an application, we consider a hypothetical idealized treatment to efficiently remove unwanted mutants by controlling the environmental conditions via the parameters K_- and ν. In this context, M cells are interpreted as unwanted mutants that have a selective advantage over the W cells we would like the population to consist of, here represented by the metapopulation consisting initially of $\Omega - 1$ demes of type W and a single M deme. In a healthy host, cells replicate in a controlled, self-regulating manner. Mutations may lead to the loss of self-regulation of cell replication, and such mutant cells replicate rapidly. This is the case of cancerous cells, that appear as rare mutants before possibly proliferating. Thus, initial conditions like those considered here are relevant, even for smaller systems. If allowed to proliferate, cancer cells will outcompete the slower-growing healthy cells, leading to a growing tumor. Therefore, in this motivating context, we wish to remove these aggressive cells while not eliminating healthy ones. The idealized treatment strategy consists of finding the set of near-optimal environmental conditions to remove M cells and minimize the risk of extinction of the entire metapopulation. This corresponds to determining the range of K_- and ν for which Φ and Θ/Θ_E are minimal. According to the above discussion, the near-optimal conditions for this idealized treatment strategy on a regular graph G are

$$\psi(m, K_-) < 1, \quad \nu \lesssim 1, \quad \nu\theta_E \gtrsim 1, \quad mK_+\theta_E \gtrsim 1. \tag{27}$$

Under these conditions, illustrated in Fig. 6, which depend on m but not on the spatial structure G, environmental variability generates a succession of strong bottlenecks at a frequency ensuring that the mutant type is the most likely to go extinct in a mean time that is much shorter than the metapopulation mean extinction time. While determining analytically Φ and Θ/Θ_E satisfying Eq. (27) is challenging, this can be done efficiently numerically as illustrated by the heatmaps of Fig. 6, and be summarized by maximizing the composite quantity

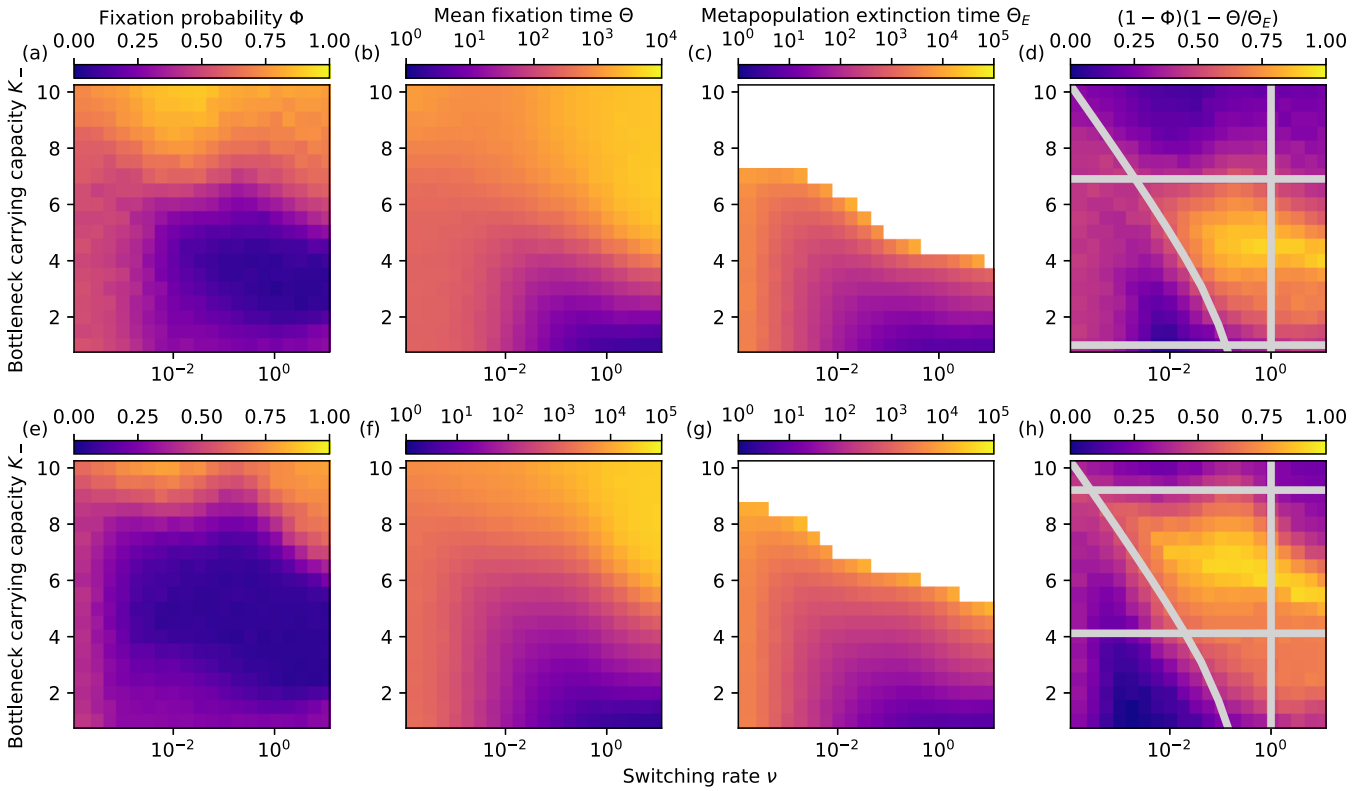

FIG. 6. Near-optimal condition for the idealized treatment strategy. (ν, K_-) heatmaps of Φ, Θ, Θ_E, and $(1-\Phi)(1-\Theta/\Theta_E)$ for a clique metapopulation. The migration rate is $m = 10^{-3}$ in panels (a)–(d) and $m = 10^{-4}$ in panels (e)–(h). White space in panels (c) and (g) indicates where at least one realization for those parameters did not reach extinction by $t = 10^5$, i.e., $\Theta_E \sim 10^5$ or larger. Gray lines in panels (d) and (h) show the near-optimal conditions for the idealized treatment strategy, given by Eq. (27): $\psi(m, K_-) < 1$ below the top horizontal line, $mK_+\theta_E > 1$ above the bottom horizontal line, and $\nu\theta_E > 1$ above the curved line, while the vertical line indicates where $\nu < 1$. Here, θ_E is obtained from Eq. (15). The near-optimal treatment conditions is the yellowish cloud at the center of the area enclosed by these lines. Similar results are obtained on other regular graphs G (see text and Fig. 10). Other parameters are $\Omega = 16$, $s = 0.1$, and $K_+ = 200$. In all panels, initially there is a single M deme and $\Omega - 1$ demes occupied by W.

$(1-\Phi)(1-\Theta/\Theta_E)$, as shown in Figs. 6(d) and 6(h). In the examples of Fig. 6, we find that the near-optimal treatment conditions are $10^{-2} \lesssim \nu \lesssim 1$ and for K_- that changes with m: $K_- \in [2, 7]$ for $m = 10^{-3}$ and $K_- \in [4, 9]$ for $m = 10^{-4}$. The idealized treatment strategy therefore consists of letting the metapopulation evolve under the near-optimal conditions [Eq. (27)], under which it undergoes a series of strong bottlenecks whose expected outcome is the removal of mutants. Once all mutants are removed, as in Fig. 5(c), the final course of the treatment consists of keeping the metapopulation in the mild environment (with $K = K_+$), where W cells would spread and finally take over all the demes. In the example of Fig. 5(c), this would be achieved by setting $K = K_+$ after $t \gtrsim 1000$. This idealized treatment strategy, illustrated for clique metapopulations in Fig. 6, qualitatively holds on regular graphs G, with small influence of the spatial structure on the shape of the heatmap when m is kept fixed, as seen by comparing Figs. 6(e)–6(h) and 10.

V. DISCUSSION, GENERALIZATIONS, AND ROBUSTNESS

Here, we discuss our main results by critically reviewing our assumptions and outline possible generalizations. We have studied the ecoevolutionary dynamics of a metapopulation consisting of Ω identical demes with the same carrying capacity K, containing wild-type W and mutant M cells, that are connected by slow migration and arranged according to regular circulation graphs. While our approach holds for any regular graph, we have specifically considered the examples of cliques (island model), cycles, and square grids (with periodic boundaries), which are all *circulation* graphs, i.e., the rate of in-flow and out-flow migration is the same at each deme. This has allowed us to consider the impact of various graph structures on the metapopulation dynamics. We have analyzed the metapopulation dynamics in a static environment where K is constant, and in a time-varying environment where K switches endlessly between K_+ and $K_- < K_+$ at a rate ν [see Eq. (6)]. In static environments, the deme size fluctuates about K and the metapopulation dynamics is characterized by either M/W competition (when $\psi \gg 1$), or by deme extinction (when $\psi < 1$). We have used suitable coarse-grained descriptions to analytically characterize the fate of the population in those regimes (see Fig. 2). When, as here, the metapopulation is spatially arranged on circulation graphs, the circulation theorem [41,47] guarantees that the fixation probability in the competition-dominated regime is independent of the migration rate and the spatial structure. We have also devised a coarse-grained three-state description of the dynamical

equilibrium in the crossover regime (where $\psi \gtrsim 1$) where in the long run there is a mixture of occupied demes of type W or M and empty demes (see Appendix F). In time-fluctuating environments, when K switches neither too quickly nor too slowly, each deme is subject to bottlenecks that can be weak when K_- is large enough to ensure $\psi(m, K_-) \gg 1$. Deme extinction can be neglected in the weak bottleneck regime, and we have combined a coarse-grained description with a PDMP approximation to characterize the W/M competition in time-varying environments in the absence of deme extinction. This has allowed us to show that weak bottlenecks lead to a *nonmonotonic* dependence of the mutant fixation probability Φ^{G} and mean fixation time Θ^{G} on the switching rate ν, with an explicit dependence on the migration rate, whereas the spatial structure has an unnoticeable effect on Φ^{G}, regardless of spatial correlations, but influences Θ^{G}. When demes are subject to strong bottlenecks, metapopulation extinction is a likely outcome under slow and fast switching ($\nu \ll 1$ and $\nu \gg 1$), whereas the overall extinction can be avoided for long periods under intermediate switching, when W/M competition and deme extinction dynamics are coupled. As a hypothetical application, we have considered an idealized treatment strategy for the rapid removal of the mutant conditioned on minimizing the risk of overall extinction.

The coarse-grained descriptions adopted in the static and dynamic environments track the dynamics of the number of M demes, which, in the case of the clique and cycle, is a single unbreakable cluster of M demes (M cluster). This requires starting from such a cluster, where we assumed the natural initial condition of a single M deme. Under these considerations, the number of active edges connecting W and M demes in cliques and cycles is known exactly, making these graphs particularly amenable to detailed analysis. It is also possible to capture the number of active edges exactly for other starting configurations of these graphs (e.g., two or more neighboring M demes) provided that the unbreakable structure of the M cluster is preserved at all times $t \geqslant 0$. For the sake of concreteness and simplicity, we have focused on a class of regular circulation graphs. In two dimensions, spatial correlations between demes are more complex, and the coarse-grained description of the M/W competition dynamics on a grid has required approximations of the number of active edges (see Appendix E). A similar approximation is expected to hold on hypercubic lattices (with periodic boundaries). These considerations on the role of the initial condition and spatial structure do not matter when the metapopulation dynamics is dominated by the extinction of demes since these occur randomly. As a consequence, the "idealized treatment strategy" based on the dynamic coupling of competition and deme extinction to remove a targeted strain is expected to hold on more complex structures, including generic regular graphs.

In this work, we have focused on the biologically relevant regime of slow migration, which is well known to increase population fragmentation and hence influences its evolution and diversity [61,87]. Here, the assumption of slow migration is crucial for the coarse-grained description of the metapopulation dynamics, and the values considered in our examples, $m \approx 10^{-5}$ to 10^{-2}, are comparable with those used in microfluidic experimental setups [63]. For $m \gg 1$, the behavior of a single well-mixed deme is recovered (see Ref. [16]. For intermediate m, the dynamics is characterized by coarsening, i.e., the slow growth of domain sizes over time [88,89]. For the sake of simplicity and without loss of generality, we have assumed that migration occurs without any directional preference and with the same rate for M and W. These assumptions can be relaxed and the coarse-grained description be readily generalized to the case of directional and type-specific migration [51], yielding the same qualitative behavior discussed here for circulation graphs. We note however that asymmetric directional migration significantly affects the evolutionary dynamics on noncirculation graphs, like the star [41,42,50,54]. It would be interesting to study the evolution on these noncirculation graphs in time-varying environments in the case of symmetric and directional migration. For computational tractability, we have chiefly considered metapopulations consisting of 16 demes of size ranging between 1 and 200, which are much smaller systems than most realistic microbial communities. However, with microfluidic devices and single-cell techniques, it is possible to perform spatially structured experiments with 10 to 100 cells per microhabitat patch, which are conditions close to those used here [63,90,91]. Moreover, *in vivo* host-associated metapopulations are often fragmented into a limited number of relatively small demes, e.g., $\Omega \approx 25$ and $K \approx 1000$ in mouse lymph nodes [60,92,93].

Here, we have conveniently represented environmental variability by the random switching of the carrying capacity $K = \{K_+, K_-\}$ driven by a symmetric dichotomous Markov noise, with the extension to asymmetric DMN outlined in Appendix H. DMN is commonly used to model evolutionary processes because it is simple to simulate and analyze, and closely reproduces the binary conditions used in many laboratory-controlled experiments. These are typically carried out in periodically changing environments [80,94,95]. It has however been shown that letting K vary periodically between K_+ and K_- with a period $1/(2\nu)$ leads to essentially the same dynamics [18]. Moreover, the relationship between DMN used here and other common forms of environmental noise has been extensively studied [18,19,70,71], showing that DMN is a convenient and nonlimiting choice to model environmental variability.

VI. CONCLUSIONS

Cells evolve in spatially structured settings, where the competition with those nearby is stronger than those further afield, subject to never-ending environmental changes. Spatial structure and environmental variability impact the eco-evolutionary dynamics of microbial populations significantly, but their joint influence is scarcely considered. Mutations frequently arise in cell communities and some may increase cell proliferation while having deleterious effects to a host organism, e.g., leading to cancerous cells or causing resistance to antibiotics [21,30–32]. Motivated by these issues, and inspired by recent advances in microfluidics allowing experiments to track dynamics at the single-cell level [63,90,91], we have investigated the classic example of a rare mutant having a selective advantage over wild-type resident cells occupying a spatially structured population in time-fluctuating environments. Here, we have considered a class of metapopulation models spatially arranged as regular (circulation)

graphs where cells of wild and mutant types compete in a *time-fluctuating* environment. The metapopulation consists of demes (subpopulations) with the same carrying capacity, connected to each other by slow cell migration. We represent environmental variability by letting the carrying capacity endlessly switch between two values associated with harsh and mild conditions. In this framework, we have studied how migration, spatial structure, and fluctuations influence the probability and time for the mutant or wild type to take over the metapopulation, and under which conditions extinction of demes and the entire metapopulation occurs. This allows us to identify when environmental variability coupled to demographic fluctuations can be utilized to remove the mutant.

We have first considered the case where demes fluctuate about a constant carrying capacity in static environments. We have thus characterized analytically and using stochastic simulations a regime dominated by the competition between the mutants and wild-type cells, another where there is deme extinction, as well as a crossover regime combining local competition and extinction. In time-varying environments, various qualitatively different dynamical scenarios arise and environmental fluctuations can significantly influence the evolution of metapopulations. When the rate of switching is neither too slow nor too fast, demes experience bottlenecks and the population is prone to fluctuations or extinction. When the fluctuating carrying capacity remains large and bottlenecks are weak, deme extinction is negligible. The dynamics is thus dominated by the competition between wild-type cells and mutants to invade and take over demes, and eventually the population, which we characterize by devising a suitable coarse-grained description of the individual-based model when migration is slow. This allows us to determine the fixation probability and mean fixation time by combining analytical and computational tools, and to show that these quantities can vary nonmonotonically with the environmental switching rate. We find that in the regime of weak bottlenecks, the mutant fixation probability on regular circulation graphs depends on the migration rate, which is in stark contrast with what happens in static environments, while the spatial structure has no noticeable influence. When the carrying capacity is small under harsh conditions, bottlenecks are strong and there is a dynamical coupling of strain competition in the mild environmental state and deme extinction in the harsh environment. This yields rich dynamical scenarios among which we identify a mechanism, expected to hold on any regular graph, driven by environmental variability and fluctuations to efficiently eradicate one strain. As a hypothetical application, we have thus proposed an idealized treatment strategy to remove the mutant, assumed to be unwanted and favored by selection. We have shown that, when each deme is subject to strong bottlenecks at intermediate switching rates, the mutant can be efficiently removed by demographic fluctuations arising in the harsh environment without exposing the entire population to a risk of rapid extinction. We have thus determined the near-optimal conditions on the switching rate and bottleneck strength for this idealized treatment strategy and found that these are qualitatively the same on other graphs.

In summary, our analysis sheds further light on the influence of the spatial structure, migration, and fluctuations on the spread of a mutant strain in time-fluctuating environments. We have identified and characterized various dynamical scenarios, displaying a complex dependence on the switching and migration rates. We have also shown how environmental variability and fluctuations can be utilized to achieve desired evolutionary outcomes like the efficient removal of a pathogenic mutant. While we have made a number of simplifying assumptions, allowing us to make analytical progress, many of these can be relaxed without affecting the results or the methodology. Our approach holds for arbitrary regular graphs and can be generalized to more complex spatial settings. We therefore believe that the model studied here has numerous potential applications. For instance, it mirrors the *in vitro* evolution of a mutant across an array of microfluidic devices, where cells migrate between "microhabitat patches" either via microchannels or pipette, with bottlenecks implemented via a strict control of the nutrient level in each device.

ACKNOWLEDGMENTS

We would like to thank K. Distefano, L. Hernández-Navarro, J. Jiménez, S. Muñoz-Montero, M. Pleimling, and A. M. Rucklidge for fruitful discussions. M.M. gratefully acknowledges funding from the U.K. Engineering and Physical Sciences Research Council (EPSRC) under the Grant No. EP/V014439/1 for the project DMS-EPSRC Eco-Evolutionary Dynamics of Fluctuating Populations [96]. The support of a Ph.D. scholarship to M.A. by the EPSRC Grant No. EP/T517860/1 is also thankfully acknowledged. M.S. and U.C.T.'s contribution to this research was supported by the U.S. National Science Foundation, Division of Mathematical Sciences under Award No. NSF DMS-2128587. This work was undertaken on ARC4, part of the High Performance Computing facilities at the University of Leeds, UK.

M.A.: Conceptualization (supporting), Formal analysis, Data curation, Investigation, Methodology, Software, Validation, Visualization, Writing original draft, and Writing review & editing. M.S.: Conceptualization (supporting), Formal analysis, Data curation, Investigation, Software, Validation, and Writing review & editing. U.C.T.: Funding acquisition, Supervision, Resources, and Writing review & editing. M.M.: Conceptualization, Formal analysis, Methodology, Validation, Funding acquisition, Supervision, Resources, Writing original draft, and Writing review & editing.

DATA AVAILABILITY

The data that support the findings of this article are openly available [97].

APPENDIX A: FURTHER DETAILS ON THE MODEL

In this Appendix, we provide further details on the model by discussing the master equation encoding its individual-based dynamics, and give further details of the size distribution of a single deme.

1. Master equation

As discussed in Sec. II, the individual-based model is a continuous-time multivariate Markov process defined by the reaction and transition rates [Eqs. (1)–(4)]. The intra- and interdeme dynamics is encoded in a master equation

(ME) for the probability $P(\{n_W, n_M\}, \xi, t)$ that at time t the metapopulation is in the environmental state ξ and configuration $\{n_W, n_M\} \equiv (\dots, n_W(x), n_M(x), \dots)$, where $n_{W/M}(x)$ denotes the number of cells of type W/M in deme $x = 1, \dots, \Omega$. The master equation for the metapopulation dynamics subject to environmental switching on a regular graph G = {clique, cycle, grid} with degrees (or number of nearest neighbors) given by $q_{\text{clique}} = \Omega - 1$, $q_{\text{cycle}} = 2$, or $q_{\text{grid}} = 4$ reads

$$\begin{aligned}\frac{\partial P(\{n_W, n_M\}, \xi, t)}{\partial t} &= \sum_{x=1}^{\Omega} \sum_{\alpha} [(\mathbb{E}_\alpha^-(x) - 1) T_\alpha^-(x) P(\{n_W, n_M\}, \xi, t) + (\mathbb{E}_\alpha^+(x) - 1) T_\alpha^+(x) P(\{n_W, n_M\}, \xi, t)] \\ &+ \frac{1}{2} \sum_{x=1}^{\Omega} \sum_{y \text{ n.n. } x} \left[(\mathbb{E}_W^+(y)\mathbb{E}_W^-(x) - 1) T_W^{m,\mathrm{G}}(x) + (\mathbb{E}_W^+(x)\mathbb{E}_W^-(y) - 1) T_W^{m,\mathrm{G}}(y)\right] P(\{n_W, n_M\}, \xi, t) \\ &+ \frac{1}{2} \sum_{x=1}^{\Omega} \sum_{y \text{ n.n. } x} \left[(\mathbb{E}_M^+(y)\mathbb{E}_M^-(x) - 1) T_M^{m,\mathrm{G}}(x) + (\mathbb{E}_M^+(x)\mathbb{E}_M^-(y) - 1) T_M^{m,\mathrm{G}}(y)\right] P(\{n_W, n_M\}, \xi, t) \\ &+ \nu [P(\{n_W, n_M\}, -\xi, t) - P(\{n_W, n_M\}, \xi, t)], \end{aligned} \tag{A1}$$

where y n.n. x denotes the sum over the q_{G} neighbors y of the deme x and $P(\dots) = 0$ whenever any of $T_\alpha^\pm$ or $T_\alpha^{m,\mathrm{G}}$ is negative. The shift operators $\mathbb{E}_\alpha^\pm(x)$ act by raising or decreasing by one the number of cells of type α in deme x. For example, $\mathbb{E}_W^\pm(x)[n_W(x)P(\dots, n_W(x), n_M(x)\dots, \xi, t)] = (n_W(x) \pm 1)P(\dots, n_W(x) \pm 1, n_M(x)\dots, \xi, t)$ and $\mathbb{E}_M^\pm(x)$ $[n_W(x)P(\dots, n_W(x), n_M(x)\dots, \xi, t)] =$ $n_W(x)P(\dots, n_W(x), n_M(x) \pm 1\dots, \xi, t)$. The first line on the right-hand side of Eq. (A1) encodes the intrademe birth-death dynamics, the second and third lines represent the interdeme dynamics via inward and outward migration, and the last line accounts for symmetric random environmental switching. Here, the ME has specifically been formulated in the presence of environmental switching, but its static-environment counterpart is readily obtained from Eq. (A1): It suffices to set $\nu = 0$ and to replace $K(t)$ by a constant carrying capacity K, yielding the ME for $P(\{n_W, n_M\}, t)$ that is the probability to find the metapopulation in a given state $\{n_W, n_M\}$ at time t (with no environmental dependence). Moreover, by setting $\Omega = 1$ and $m = 0$ in Eq. (A1), the second and third lines on the RHS cancel, we obtain the ME encoding the intrademe dynamics of a single isolated deme [16,17].

While the ME [Eq. (A1)] holds for any regular graphs G, in our examples we consider specifically the regular circulation graphs G = {clique, cycle, grid}. The space-dependent individual-based dynamics encoded in the ME [Eq. (A1)] has been simulated using the Monte Carlo method described in Appendix I. It is worth noting that demographic fluctuations eventually lead to the extinction of the entire metapopulation, in all regimes. However, this phenomenon occurs after a time growing dramatically with the system size, and it can generally not be observed in sufficiently large metapopulations [see Fig. 2(b), bottom right].

2. Ecoevolutionary dynamics of a single deme

Since the metapopulation consists of a graph of connected demes, all with the same carrying capacity, we can gain significant insight into its dynamics by looking into its building block. In this section, we therefore analyse the ecoevolutionary dynamics of a single isolated deme (when $m = 0$).

For an isolated deme, there is only intrademe dynamics according to the birth-death process defined by Eqs. (1) and (2). The ME for the dynamics of a single isolated deme is thus given by setting $\Omega = 1$ and $m = 0$ in Eq. (A1) (see Appendix A 1). The corresponding intrademe dynamics in a time-varying environment can be simulated using exact methods like the Gillespie algorithm [98], as in Refs. [16–18,20–24]. It is instructive to ignore all forms of fluctuations and consider the mean-field approximation of an isolated deme dynamics subject to a constant carrying capacity $K \gg 1$. Following Refs. [16,17], with the transition rates [Eq. (2)], the mean-field ecoevolutionary dynamics of a single isolated deme is characterized by rate equations for the size n of the deme and the fraction $x = n_M/n$ of mutants in the deme, which read

$$\begin{aligned}\dot{n} &= \sum_\alpha T_\alpha^+ - \sum_\alpha T_\alpha^- = n\left(1 - \frac{n}{K}\right), \\ \dot{x} &= \frac{T_M^+ - T_M^-}{n} - x\frac{\dot{n}}{n} = \frac{sx(1-x)}{1+sx}, \end{aligned} \tag{A2}$$

where the dot indicates the time derivative and we have used $f_M = 1 + s$ and $f_W = 1$. The prefactors of these decoupled rate equations predict the relaxation of the deme size toward the constant carrying capacity, with $n \to K$ on a timescale $t \sim 1$, and the growth of the fraction of mutants, with $x \to 1$ on a timescale $t \sim 1/s$. In the total absence of fluctuations, when $0 < s \ll 1$ (small selective advantage to M), in the mean-field picture, the deme size quickly approaches the carrying capacity and there is a timescale separation between n and x, respectively, the fast and slow variables, where n evolves on a timescale of order 1 and x on a timescale $\sim 1/s \gg 1$ (see Table I). Thus, W cells are thus slowly wiped out by mutants that take over the deme on a timescale $t \sim 1/s \gg 1$ [16,17]. It is worth noting that with the effective transition rates [Eq. (21)], we have assumed that invasions always occur after deme size and composition relaxation. This means that Eqs. (25) and (26) assume a timescale separation between n and x in addition to the slow migration assumption.

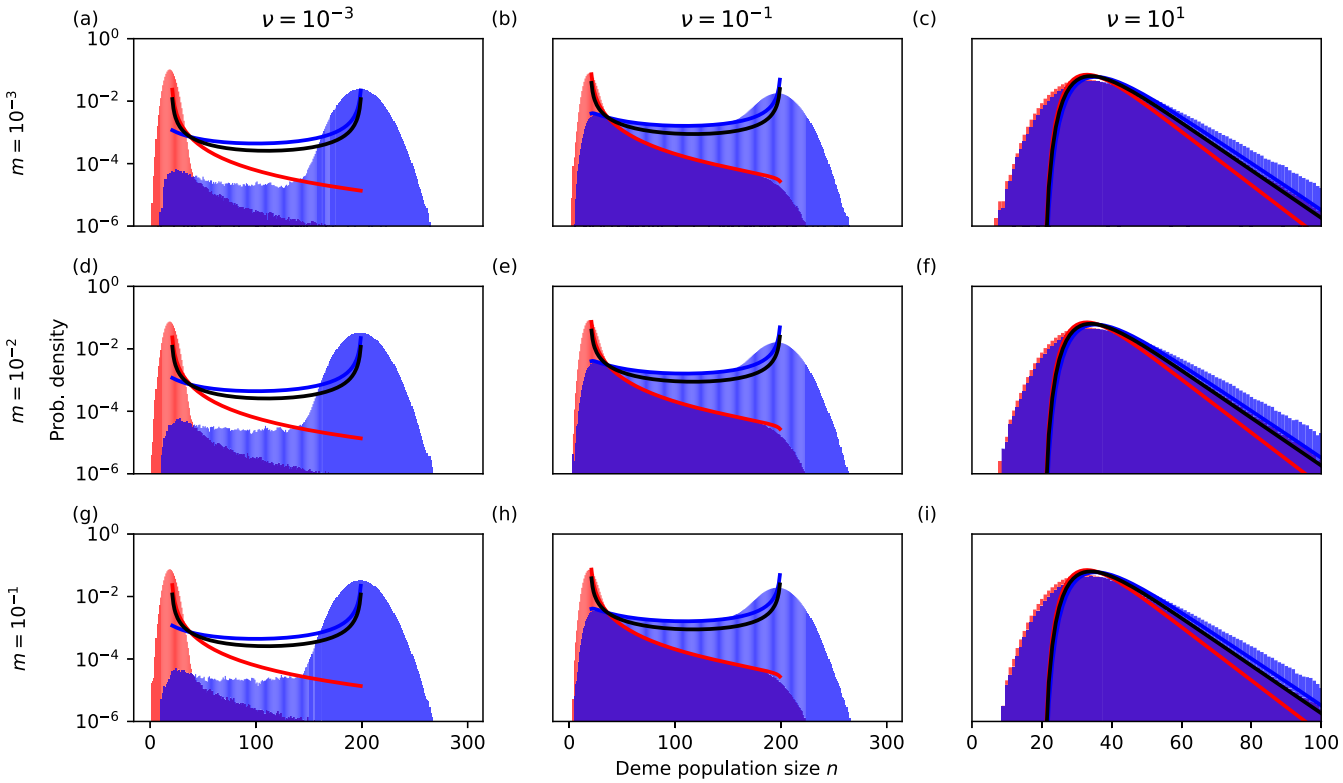

FIG. 7. Quasistationary probability density of deme population size (n-QPSD) distribution on clique metapopulations for various parameters and its n-PDMP approximation given by Eqs. (19) and (A4). Red and blue bars show data for the n-QPSD conditioned on $K(t) = K_-$ and $K(t) = K_+$, respectively. Red, blue, and black solid lines are the n-PDMP stationary densities $p_-(n;\nu)$, $p_+(n;\nu)$, and $p(n;\nu)$, respectively, given by Eqs. (19) and (A4). Panels (a)–(c) are for $m = 10^{-3}$, (d)–(f) for $m = 10^{-2}$, and (g)–(i) for $m = 10^{-1}$. We have $\nu = 10^{-3}$ in panels (a), (d), and (g), $\nu = 10^{-1}$ in panels (b), (e), and (h), and $\nu = 10^{2}$ in panels (c), (f), and (i). Other parameters are $\Omega = 16$, $K_+ = 200$, and $K_- = 20$. All represent a single realization tracked until $t = 10^5$.

It is also relevant to consider the intrademe dynamics of a single isolated site subject to a finite constant carrying capacity K. As explained in Appendix B, the intrademe dynamics can be well approximated by a Moran process for a deme of constant size $n = K$ [7,16,17,64–66], and characterized by the fixation probability and mean fixation time given by Eq. (B3). The probability $\rho_{M/W}(K)$ that a single M/W cell takes over a W/M deme of size K is given by Eq. (10).

When demographic fluctuations can be neglected and randomness only arises from environmental variability via Eq. (6), the intrademe dynamics of an isolated deme is well captured by the piecewise deterministic Markov process (PDMP) for n, obtained by ignoring demographic fluctuations [16,17,85]. In the realm of the PDMP approximation, the deme size thus satisfies a deterministic logistic equation in each environmental state, subject to a carrying capacity that switches when the environment changes ($K = K_\pm$ when $\xi = \pm 1$), yielding the n-PDMP [16–18,21,22,32]

$$\dot{n} = \begin{cases} n\left(1 - \frac{n}{K_-}\right) & \text{if } \xi = -1, \\ n\left(1 - \frac{n}{K_+}\right) & \text{if } \xi = +1, \end{cases} \tag{A3}$$

that is decoupled from the mean-field equation for x that is as in Eq. (A2). The stationary joint probability density of this n-PDMP is given by Eq. (19) [17,18], while the marginal probability density is

$$p(n;\nu) = \frac{1}{2}\sum_{\xi} p_\xi(n;\nu) = \frac{\mathcal{Z}}{n^2}\left[\left(\frac{K_+}{n} - 1\right)\left(1 - \frac{K_-}{n}\right)\right]^{\nu-1}, \tag{A4}$$

where $\mathcal{Z}$ is the normalization constant and $n \in [K_-, K_+]$. Despite ignoring the effect of demographic noise, $p(n;\nu)$ aptly captures many properties of the quasistationary distribution of the size of an isolated single deme [17,18]. For instance, the long-time average deme size is accurately approximated by $\mathcal{N}(\nu) = \int_{K_-}^{K_+} n p(n;\nu) \mathrm{d}n$, and is a decreasing function of ν [16,17].

While $p_\xi(n;\nu)$ and $p(n;\nu)$ give a PDMP description of the quasistationary distribution of the size of an isolated deme ($m = 0$), the n-PDMP stationary densities given by Eqs. (19) and (A4) are still a valid approximation of the long-time size distribution of n in the presence of migration between many connected demes, as considered here. In fact, as shown below in Fig. 7, the influence of migration on the distribution of the deme size is essentially unnoticeable, where the predictions of Eqs. (19) for a single isolated deme (no migration) are compared with the deme size distribution obtained by sample averaging across all demes of the metapopulation in the presence of migration. Its main features are therefore well captured by Eqs. (19) and (A4). As illustrated by Fig. 7, the density $p(n;\nu)$ correctly predicts that the deme size distribu-

tion is bimodal when $\nu < 1$ and unimodal when $\nu > 1$, and that it is peaked at $n \approx K_\pm$ when $\nu \ll 1$ (slow switching) and centered around $n \approx \mathcal{K}$ when $\nu \gg 1$ (fast switching) [see Eq. (17)]. The joint and marginal PDMP probability densities Eqs. (19) and (A4) provide valuable insight into the deme size distribution when these are subject to weak bottlenecks and their extinction can be neglected [16–19,21,22,32].

In the main text, we have used the PDMP approximation to describe the size distribution of a single isolated deme subject to symmetric random switching of its carrying capacity [Eq. (6)]. Here, we show that spatial migration has no noticeable influence on the size distribution of a single deme of a metapopulation structured as a clique (though the same holds for other spatial structures). To this end, in Fig. 7, we compare the size distribution of a single deme in a metapopulation structured as a clique in the presence of a migration per capita rate $m \in \{10^{-3}, 10^{-2}, 10^{-1}\}$ (obtained from stochastic simulations) with the predictions of Eq. (19). These results illustrate that migration has no noticeable effect on the deme size distribution that can approximated by PDMP density Eq. (19) [or Eq. (A4)] in the absence and presence of migration.

As a consequence, the deme size distribution of any metapopulation considered here is well approximated by the joint and marginal PDMP densities $p_\pm(n;\nu)$ and $p(n;\nu)$, given by Eqs. (19) and (A4).

Intuitively, this can be understood by noting that the spatial structures considered here are circulation graphs, yielding the same inward and outward migration flow at each deme, and each deme has the same carrying capacity. As a consequence, the average number of cells per deme is expected to be independent of migration. The latter remains well captured by $p_\pm(n;\nu)$ and $p(n;\nu)$ regardless of migration rate, as seen in Fig. 7.

APPENDIX B: DEME INVASION

In this Appendix, we analyze the process of invasion of a single deme subject to a constant carrying capacity K when $\psi(m,K) \gg 1$ (see Sec. III A). In this competition-dominated regime, the extinction of demes can be neglected and their size rapidly fluctuates about K [see Fig. 1(a)]. In this scenario, we can assume that the deme size is constant $n(x) = K$, and describe the deme dynamics by tracking the number of mutants n_M and wild-type cells n_W in the deme x. The deme composition $(n_M, n_W) = (n_M, K - n_M)$ thus changes according to the Moran process [7,64–66]

$$\begin{aligned}(n_M, n_W) &\xrightarrow{\mathcal{T}^+_{\mathrm{Mo}}} (n_M + 1, n_W - 1),\\ (n_M, n_W) &\xrightarrow{\mathcal{T}^-_{\mathrm{Mo}}} (n_M - 1, n_W + 1),\end{aligned} \tag{B1}$$

where the transition rates are defined in terms of $T^\pm_{M/W}$, given by Eq. (2), according to [16,17,21,22]

$$\begin{aligned}\mathcal{T}^+_{\mathrm{Mo}}(n_M) &= \frac{T^+_M T^-_W}{K} = \frac{f_M}{\overline{f}}\frac{n_M n_W}{K} = \frac{f_M}{\overline{f}} n_M\Big(1 - \frac{n_M}{K}\Big),\\ \mathcal{T}^-_{\mathrm{Mo}}(n_M) &= \frac{T^-_M T^+_W}{K} = \frac{f_W}{\overline{f}}\frac{n_M n_W}{K} = \frac{f_W}{\overline{f}} n_M\Big(1 - \frac{n_M}{K}\Big).\end{aligned} \tag{B2}$$

These transition rates correspond to the effective rates of increase and decrease in the number of M in a deme of size K. This Moran process conserves the deme size by accompanying each birth of an M/W by the simultaneous death of a W/M, and is characterized by the absorbing states $(n_M, n_W) = (K, 0)$ (M deme) and $(n_M, n_W) = (0, K)$ (W deme). The M fixation probability ϕ_{Mo} and unconditional mean fixation time θ_{Mo} for this Moran process are classical results, and when there are initially i cells of type M, they read [7,65–67]

$$\begin{aligned}\phi_{\mathrm{Mo}}(i) &= \frac{1 - \gamma^i_{\mathrm{Mo}}}{1 - \gamma^K_{\mathrm{Mo}}},\\ \theta_{\mathrm{Mo}}(i) &= \phi_{\mathrm{Mo}}(i)\sum_{n=i}^{K-1}\sum_{l=1}^{n}\frac{\gamma^{n-l}_{\mathrm{Mo}}}{\mathcal{T}^+_{\mathrm{Mo}}(l)}\\ &\quad - (1 - \phi_{\mathrm{Mo}}(i))\sum_{n=1}^{i-1}\sum_{l=1}^{n}\frac{\gamma^{n-l}_{\mathrm{Mo}}}{\mathcal{T}^+_{\mathrm{Mo}}(l)},\end{aligned} \tag{B3}$$

where $\gamma_{\mathrm{Mo}} \equiv \mathcal{T}^-_{\mathrm{Mo}}/\mathcal{T}^+_{\mathrm{Mo}} = f_W/f_M = 1/(1+s)$. The fixation probability of a single mutant ($i = 1$) and of a single W cell ($i = K - 1$) are particularly relevant for our purposes, and explicitly read

$$\begin{aligned}\rho_M &\equiv \phi_{\mathrm{Mo}}(1) = \frac{s}{1+s}\left[\frac{1}{1 - (1+s)^{-K}}\right],\\ \rho_W &\equiv 1 - \phi_{\mathrm{Mo}}(K-1) = \frac{s}{(1+s)^K}\left[\frac{1}{1 - (1+s)^{-K}}\right].\end{aligned} \tag{B4}$$

APPENDIX C: DEME AND METAPOPULATION MEAN EXTINCTION TIMES

In this Appendix, we discuss the process of extinction of a single deme that has a constant carrying capacity K when $\psi(m,K) \ll 1$ (see Sec. III B). In this extinction-dominated regime, we can assume that the deme size rapidly fluctuates about K, and extinction occurs from a deme of constant size $n(x) = K$ prior to any invasion. Without loss of generality (see below), we hence assume that extinction occurs from entirely occupied demes, with the metapopulation consisting only of W and M demes, all of size K. In this representation, the dynamics of a W/M deme when $\psi \ll 1$ is given by the birth-death process of Sec. II with transition rates $T^+_{W/M} = n_{W/M}$ and $T^-_{W/M} = n^2_{W/M}/K$, subject to an absorbing boundary at $n_{W/M} = 0$ [see Eq. (2)]. Clearly therefore, the deme dynamics is independent of its type, and the deme mean extinction time is the average time to reach $n_{W/M} = 0$ and is the same for W and M demes (dMET is independent of s). A classical calculation (see, e.g., Sec. 6.7 in Ref. [73]) for an initially fully occupied deme of size K yields

$$\tau_E(K) = \sum_{n=0}^{K-1}\left(\frac{n!}{K^n}\sum_{i=n+1}^{\infty}\frac{1}{i}\frac{K^i}{i!}\right). \tag{C1}$$

The leading contribution to this expression arises from the term $n = 0$: $\tau_E(K) \simeq \sum_{i=1}^{\infty} K^i/(i \cdot i!)$. This expression, corresponding to the dMET of a deme initialized with a single cell (of either type), is a good approximation of Eq. (C1) that indicates that the dMET is independent of selection and initial condition (for the leading order of τ_E). We can further

simplify the leading contribution to the dMET by writing

$$\begin{aligned}\tau_E(K) &\simeq \sum_{n=1}^{\infty} \frac{K^n}{n!} \int_0^1 t^{n-1} \mathrm{d}t, \\ &= \int_0^1 \frac{1}{t} \sum_{n=1}^{\infty} \frac{(Kt)^n}{n!} \mathrm{d}t, \\ &= \int_0^K \frac{e^u - 1}{u} \mathrm{d}u,\end{aligned}$$

where we have used $u = Kt$. The main contribution to the last integral stem from the upper bound, yielding

$$\tau_E(K) \simeq \frac{e^K}{K}. \tag{C2}$$

The dMET hence increases almost exponentially with K and is independent of the deme type and its initial state.

The metapopulation mean extinction time in the regime $\psi(m, K) \ll 1$ can be obtained analytically within the realm of the above coarse-grained description, in the spirit of the approach of Ref. [59] for cliques. The metapopulation thus consists initially of entirely occupied demes (i mutant demes and $\Omega - i$ type W demes). Since deme extinction here occurs prior to any invasion, we describe the metapopulation dynamics in terms of the number $j = 0, 1, \ldots, \Omega$ of entirely occupied demes. Residents (of either W or M type) of these filled demes can recolonize a neighboring empty site at a rate $B(j)$ [see Fig. 1(d)]. In addition, each occupied deme goes extinct at a rate $D(j)$. This coarse-grained description of the metapopulation dynamics is therefore a birth-death process with an absorbing state $j = 0$ corresponding to the eventual extinction of the metapopulation, and a reflecting boundary at $j = \Omega$ (all demes are occupied). In this picture, proceeding as above [73], the mMET reads

$$\theta_E(K, \Omega) = \sum_{n=1}^{\Omega-1} \left[\left(\prod_{m=1}^{n-1} \frac{B(m)}{D(m)} \right) \sum_{j=n}^{\Omega} \frac{\prod_{l=1}^{j} \frac{B(l)}{D(l)}}{D(j)} \right]. \tag{C3}$$

In the vein of Ref. [59], the recolonization-birth rate of occupied demes is $B(j) = mKj(1 - j/\Omega)$, corresponding to a logistic growth with a rate proportional to the expected number of migrations from an occupied deme mK. Here, the extinction rate is $D(j) = j/\tau_E$ and is inversely proportional to the mean local extinction time, that is the dMET. With $\psi = mK\tau_E$, using $\prod_{l=n}^{j-1}(1 - \frac{l}{\Omega}) = \frac{1}{\Omega^{j-n}} \frac{(\Omega-n)!}{(\Omega-j)!}$, Eq. (C3) can be rewritten as

$$\theta_E(K, \Omega) = \tau_E(K) \sum_{n=1}^{\Omega} \sum_{j=n}^{\Omega} \frac{1}{j} \left(\frac{\psi}{\Omega} \right)^{j-n} \frac{(\Omega - n)!}{(\Omega - j)!}. \tag{C4}$$

In the extinction-dominated regime $\psi \ll 1$, the main contribution to the inner sum stems from $j = n$, and the leading contribution to the mMET is therefore

$$\theta_E(K, \Omega) \approx \tau_E(K) \sum_{n=1}^{\Omega} \frac{1}{n} = \tau_E(K) H_\Omega, \tag{C5}$$

where H_Ω is the Ωth harmonic number. Asymptotically, we have $H_\Omega \simeq \ln(\Omega) + \gamma_{\mathrm{EM}} + \mathcal{O}(\Omega^{-1})$ where $\gamma_{\mathrm{EM}} \approx 0.577...$ is the Euler-Mascheroni constant. This expression is independent of selection and, to leading order, generally does not depend on the initial state of the metapopulation. In the limit of a large metapopulation, $\Omega \gg 1$, the metapopulation mean extinction time in the regime $\psi(m, K) \ll 1$, is asymptotically given by the simple expression Eq. (15): $\theta_E(K, \Omega) \simeq \tau_E(\ln(\Omega) + \gamma_{\mathrm{EM}})$. When $\Omega \gg 1$ and $K \gg 1$, we simply have $\theta_E(K, \Omega) \simeq e^K \ln(\Omega)/K$.

The result $\theta_E(K, \Omega)$ has been explicitly derived for cliques (island model), but is found to provide good qualitative insight into the extinction dynamics for cycles and grids (see Fig. 2).

APPENDIX D: STATIONARY DEME OCCUPANCY

In the realm of the coarse-grained description of the extinction-dominated regime discussed in the previous Appendix, we can use the rates $B(j) = mKj(1 - j/\Omega)$ and $D(j) = j/\tau_E$ to estimate the number of occupied demes Ω_{occ} in the metapopulation when the environment is static (constant carrying capacity K). At mean-field level, we can write the following balance equation [35]:

$$\begin{aligned}\frac{\mathrm{d}}{\mathrm{d}t}\Omega_{\mathrm{occ}} &= B(\Omega_{\mathrm{occ}}) - D(\Omega_{\mathrm{occ}}) \\ &= mK\Omega_{\mathrm{occ}} \left(1 - \frac{1}{\psi} - \frac{\Omega_{\mathrm{occ}}}{\Omega} \right).\end{aligned} \tag{D1}$$

The equilibria of this equation are $\Omega_{\mathrm{occ}} = 0$ and $\Omega_{\mathrm{occ}} = \Omega \frac{\psi - 1}{\psi}$ when $\psi > 1$. The equilibrium $\Omega_{\mathrm{occ}} = 0$ is asymptotically stable when $\psi < 1$ and unstable otherwise. This means that all demes go extinct, and there is extinction of the entire metapopulation when $\psi < 1$. When $\psi > 1$, the equilibrium $\Omega_{\mathrm{occ}} = \Omega \frac{\psi - 1}{\psi}$ is asymptotically stable. This corresponds to a fraction $1 - 1/\psi$ of the demes being entirely occupied, and there is fraction $1/\psi$ of empty demes. In the limit where $\psi \gg 1$, we have $\Omega_{\mathrm{occ}} \to \Omega$ and all demes and hence the metapopulation are fully occupied. Putting everything together, we obtain Eq. (9).

This mean-field derivation of Ω_{occ} is accurate for large clique metapopulations but, as it ignores spatial correlations, it is a crude approximation for cycles and grids (see Fig. 9). In particular, Ω_{occ} overestimates the number of occupied demes in cycles when ψ is not much larger than 1. However, $\psi = mK\tau_E$ allows us to distinguish between different regimes and provides a sound estimate of the number of occupied demes in the intermediate regime when $\psi(m, K) \approx me^K$ is sufficiently bigger than 1.

APPENDIX E: AVERAGE NUMBER OF ACTIVE EDGES ON THE SQUARE GRID AND THE INFLUENCE OF THE SPATIAL STRUCTURE

In principle, the coarse-grained description of the M/W competition holds for any regular circulation graph. However, this approach requires the number of active edges for a given number of mutant demes to be known, which, except for cycles (one dimension) and cliques, is a difficult task due to complex spatial correlations between demes. Here, we consider the case of the square grid (with periodic boundaries), and illustrate how to estimate the average number of active edges when the metapopulation consists of only one single fully occupied M deme and all other demes are occupied by W cells. In the case of a large metapopulation, $\Omega \gg 1$, with

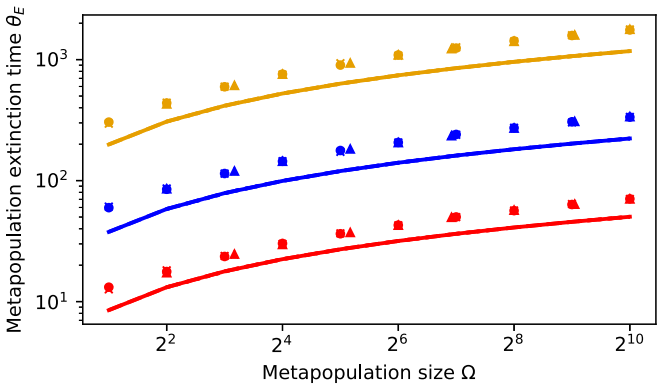

FIG. 8. θ_E vs metapopulation size Ω for $K = 7$ (yellow), $K = 5$ (blue), $K = 3$ (red) and $m = 10^{-4}$. Markers are simulation results and lines are predictions of Eq. (C4) for cliques (solid lines/crosses), cycles (dashed lines/circles), and grids (dotted lines/triangles). For the grid, the values of Ω are chosen to maintain a square lattice, and thus occasionally differ slightly from the metapopulation size used in the cycle and clique. Markers of the same color are almost indistinguishable. Deviations occur due to the approximation of $\tau_E(K)$ in Eq. (C2). Selection plays no role in this regime, so results have been obtained with $s = 0$.

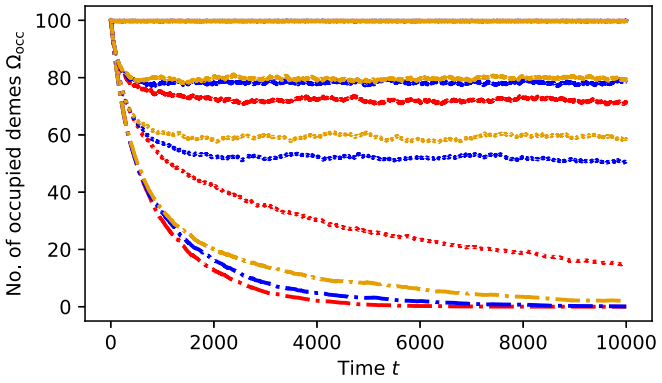

FIG. 9. Metapopulation occupancy: Ω_{occ} vs t for cliques (yellow), cycles (red), and grids (blue), with $\Omega = 100$ and $K = 8$. Simulation results averaged on 100 realizations for the stationary number Ω_{occ} of occupied demes for $\psi = 100$ (solid lines), $\psi = 5$ (dashed lines), $\psi = 2.5$ (dotted lines), and $\psi < 1$ (dash–dotted lines). Equation (9) predicts $\Omega_{occ} = 100, 80, 60,$ and 0 for $\psi = 100, 5, 2.5,$ and $\psi < 1$, respectively.

unit spacing between neighbors, we assume that the mutant spreads outward from the initial M deme approximately forming an M cluster with a circular front. If this circular M cluster has a radius r, it has an area πr^2 containing a number i of M demes. The boundary of the circular M cluster is of length $2\pi r$. Assuming that this length is equal to the number of M demes on the boundary, we find that $r = \sqrt{i/\pi}$ and there are $2\sqrt{i\pi}$ boundary demes given i demes of type M. We therefore estimate that the average number active edges for a grid is $E_{\text{grid}}(i) \approx 2\sqrt{\pi i}$. We have notably used this approximation in the transitions rates [Eqs. (11) and (21)] for the coarse-grained description of M/W competition in static and time-varying environments in the regime of weak bottlenecks.

In Figs. 2(a) (top) and 4(c), we have found that the spatial structure has a barely noticeable influence on the fixation probability under both constant carrying capacity and in the regime of weak bottlenecks. The mean fixation time also appears unchanged when the carrying capacity is constant. Figure 10 shows the heatmaps on a cycle and a grid metapopulation for the "idealized treatment strategy" proposed in Sec. IV B, which are almost identical. This is in accord with Eq. (27) predicting that the same migration rate yields the same near-optimal conditions for the heatmaps of metapopulation on any regular graph, here a cycle and a grid. Simulation results confirm spatial structure is only responsible for minor quantitative changes in the region of the heatmaps corresponding to the near-optimal "treatment conditions." This stems from the removal scenario characterizing the idealized treatment strategy being due to deme extinction that is mostly independent of G and m.

APPENDIX F: INTERMEDIATE DYNAMICS IN STATIC ENVIRONMENTS

When $\psi \gtrsim 1$ with $mK < 1$ (slow migration) in static environments, migration and deme extinction occur on the timescale τ_E. In the long run, deme recolonizations and extinctions balance each other, yielding a dynamical equilibrium consisting of $\Omega_{occ} = \Omega(1 - 1/\psi)$ occupied demes and $\Omega - \Omega_{occ}$ empty demes (see Fig. 9). In this regime, the three-state coarse-grained description of the dynamical equilibrium consists of a random mixture of empty demes, and occupied W and M demes [see Fig. 1(d)]. After a mean time $\theta^{\text{G}}_{\text{int}}$, the metapopulation reaches the dynamical equilibrium consisting of a fraction $1 - \Omega_{occ}/\Omega = 1/\psi$ empty demes, and the remaining demes are all of either type M or W with probability $\phi^{\text{G}}_{\text{int}}$ and $1 - \phi^{\text{G}}_{\text{int}}$, respectively. The dynamical equilibrium is thus defined by the quantities ψ, given by Eq. (8), and $\phi^{\text{G}}_{\text{int}}$ that is the probability that mutants M take over the $\Omega_{occ} = \Omega(1 - 1/\psi)$ occupied demes, where the unconditional mean fixation time is given by $\theta^{\text{G}}_{\text{int}}$. In this Appendix, we complete the results given in the main text by considering metapopulation intermediate dynamics on a regular graph G, obtaining the explicit results $\phi^{\text{G}}_{\text{int}}$ and $\theta^{\text{G}}_{\text{int}}$ for G = {clique, cycle, grid} reported in Fig. 11 when the metapopulation initially consists of a single M deme and $\Omega - 1$ demes occupied by W. This region is concretely defined for values of ψ such that $1 < \psi < K\Omega$ for $\Omega \gg 1$, where the lower bound ensures $\Omega_{occ} = 1$ from Eq. (9) and the upper bound is obtained by considering the limiting case where every individual is expected to migrate on the timescale of deme extinction. Using that $\psi \approx me^K$ for $K \gg 1$, we obtain the condition $\ln(1/m) \lesssim K \lesssim \ln(K\Omega/m)$. These bounds are illustrated by the vertical lines in Fig. 11.

The intermediate regime is characterized by M/W competition and deme extinction. Therefore, in addition to invasions, a W deme may become an M deme through extinction followed by a recolonization, i.e., $W \to \emptyset \to M$, where $\emptyset$ indicates an extinct deme. Similarly, an M deme can be changed into a W deme via $M \to \emptyset \to W$. We assume that there is initially a single M deme in the metapopulation (and $\Omega - 1$ demes of type W). With a probability p_{surv} (see below), the initial M deme survives the short transient as the metapopulation reaches the dynamical equilibrium that consists of the M deme, the remaining W demes, and extinct demes. The

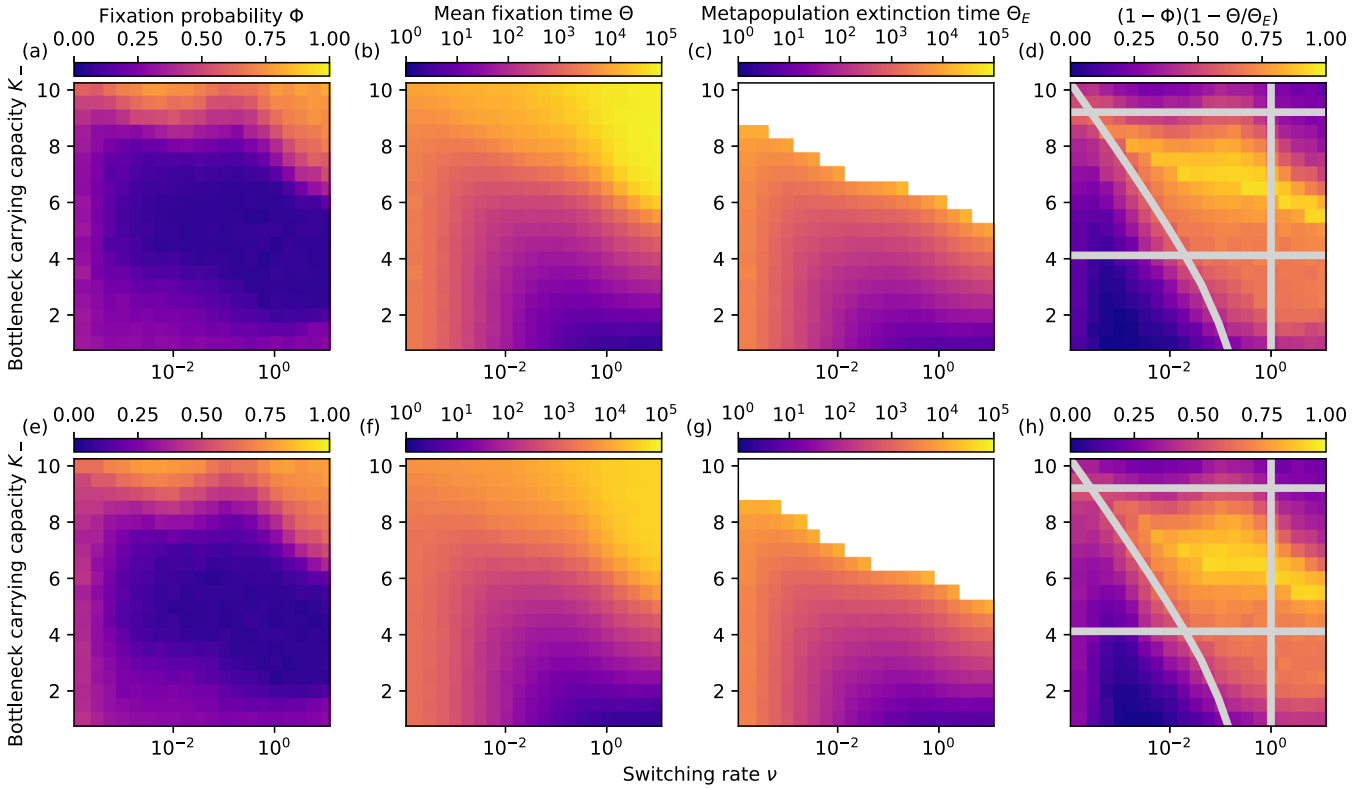

FIG. 10. Near-optimal condition for the idealized treatment strategy on a cycle and grid metapopulation. (ν, K_-) heatmaps of Φ, Θ, Θ_E, and $(1-\Phi)(1-\Theta/\Theta_E)$ for (a)–(d) the cycle and (e)–(h) grid metapopulations (see Appendix E). White space in panels (c) and (g) indicates the parameter region where at least one realization for those parameters did not reach extinction by $t = 10^5$. Gray lines in panels (d) and (h) show the near-optimal conditions for the idealized treatment strategy: $\psi(m, K_-) < 1$ below the top horizontal line, $mK_+\theta_E > 1$ above the bottom horizontal line, and $\nu\theta_E > 1$ above the curved line, while the vertical line indicates where $\nu < 1$ and θ_E from Eq. (15). The near-optimal treatment conditions is the yellowish cloud at the center of the area enclosed by these lines. Other parameters are $\Omega = 16$, $m = 10^{-4}$, $s = 0.1$, and $K_+ = 200$. In all panels, initially there is a single M deme and $\Omega - 1$ demes occupied by W.

number of M demes $i = 0, 1, \ldots, \Omega_{\rm occ}$ grows and shrinks through invasions and extinction-recolonization events. We assume that immediately $\Omega_E = \Omega/\psi$ demes go extinct, so that the metapopulation quickly reaches its equilibrium occupancy $\Omega_{\rm occ} = \Omega(1 - 1/\psi)$. In this dynamical equilibrium, a W deme can become an M deme via $W \to \emptyset$ (W deme extinction) at rate $r_{{\rm ext},W}$ followed by $\emptyset \to M$ (recolonization by M) at rate $r^{\rm G}_{{\rm rec},M}$. The overall extinction-recolonization reaction $W \to \emptyset \to M$ thus occurs at rate $1/(1/r_{{\rm ext},W} + 1/r^{\rm G}_{{\rm rec},M})$. Here, the rate of W deme extinction is $r_{{\rm ext},W} = (\Omega_{\rm occ} - i)/\tau_E$ and τ_E is given by Eq. (7). We proceed similarly for the extinction of an M deme and its recolonization into a W site according to $M \to \emptyset \to W$. Taking also into account the rate of invasion [see Eq. (11)], the number of M demes i on a regular graph G varies according to the transition rates

$$\widetilde{T}^+_i(m, {\rm G}, K) = mK\frac{\widetilde{E}_{\rm G}(i)}{q_{\rm G}}\left[\rho_M + \frac{1}{\psi - 1}\frac{q_{\rm G}}{\Omega}\frac{i(\Omega_{\rm occ} - i)}{\widetilde{E}_{\rm G}(i)}\right],$$
$$\widetilde{T}^-_i(m, {\rm G}, K) = mK\frac{\widetilde{E}_{\rm G}(i)}{q_{\rm G}}\left[\rho_W + \frac{1}{\psi - 1}\frac{q_{\rm G}}{\Omega}\frac{i(\Omega_{\rm occ} - i)}{\widetilde{E}_{\rm G}(i)}\right]. \quad \text{(F1)}$$

It is important to note that the $\widetilde{E}_{\rm G}(i)$ in these expressions explicitly represent the number of active edges between M and W on the metapopulation given i mutant demes, taking into account the presence of extinct demes. Therefore, their expressions for a given graph structure G generally differ from those considered in the competition-dominated regime, denoted $E_{\rm G}(i)$. With these rates, we can solve the following first-step analysis equations for the probability $\phi^{\rm G}_{{\rm int},i}$ that the dynamical equilibrium comprising initially i demes of type M consists of occupied M demes and extinct demes after a mean time $\theta^{\rm G}_{{\rm int},i}$:

$$(\widetilde{T}^+_i + \widetilde{T}^-_i)\phi^{\rm G}_{{\rm int},i} = \widetilde{T}^+_i\phi^{\rm G}_{{\rm int},i+1} + \widetilde{T}^-_i\phi^{\rm G}_{{\rm int},i-1},$$
$$(\widetilde{T}^+_i + \widetilde{T}^-_i)\theta^{\rm G}_{{\rm int},i} = 1 + \widetilde{T}^+_i\theta^{\rm G}_{{\rm int},i+1} + \widetilde{T}^-_i\theta^{\rm G}_{{\rm int},i-1}. \quad \text{(F2)}$$

These equations are subject to the boundary conditions $\phi^{\rm G}_{{\rm int},0} = 0$, $\phi^{\rm G}_{{\rm int},\Omega_{\rm occ}} = 1$ and $\theta^{\rm G}_{{\rm int},0} = \theta^{\rm G}_{{\rm int},\Omega_{\rm occ}} = 0$. We thus have $\phi^{\rm G}_{\rm int} \equiv p_{\rm surv}\phi^{\rm G}_{{\rm int},1}$ and $\theta^{\rm G}_{\rm int} \equiv p_{\rm surv}\theta^{\rm G}_{{\rm int},1} + (1 - p_{\rm surv})\tau_E$. The factor $p_{\rm surv} = \frac{\Omega_{\rm occ}}{\Omega} = 1 - 1/\psi$ is the probability that the initial M deme reaches the dynamical equilibrium (after what is assumed to be a short transient), while the contribution $(1 - p_{\rm surv})\tau_E$ to $\theta^{\rm G}_{\rm int}$ accounts for the probability that the initial M deme goes extinct in a mean time τ_E [given by Eq. (7)]

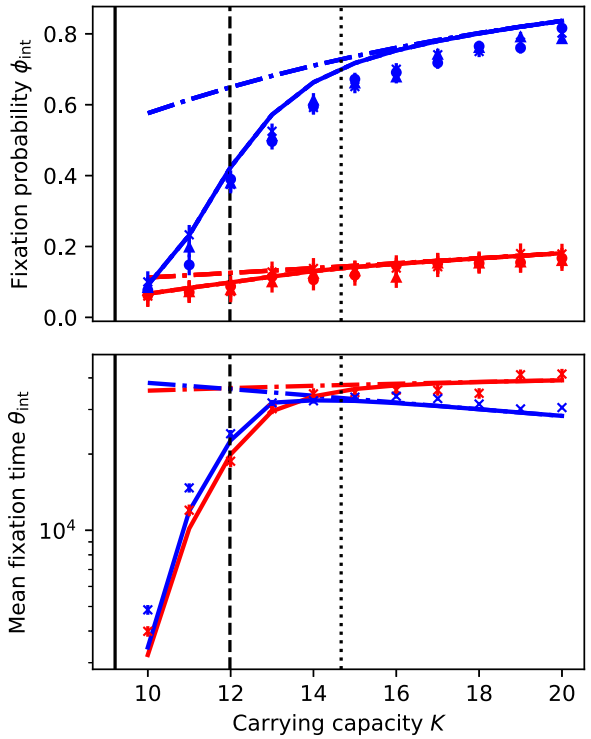

FIG. 11. $\phi_{\rm int}$ vs K for $s = 0.1$ (blue) and $s = 0.01$ (red) on clique (solid lines/crosses), cycle (dashed lines/circles), and a grid (dotted lines/triangles). The different symbols and lines are almost indistinguishable. $\theta_{\rm int}$ vs K for the same parameters for a clique metapopulation. The vertical solid and dashed line indicate where the number of occupied demes $\Omega_{\rm occ} \in [1, \Omega - 1]$ (see text). The dotted line indicates where $\psi = K\Omega$, i.e., every individual migrates in the time required for an independent deme extinction. Markers show simulation results, solid lines are predictions of Eq. (F3), and dash–dotted lines are predictions of Eq. (14). Other parameters are $m = 10^{-4}$ and $\Omega = 16$.

before reaching the equilibrium. The final expressions of $\phi_{\rm int}^{\rm G}$ and $\theta_{\rm int}^{\rm G}$ thus read

$$\phi_{\rm int}^{\rm G} = p_{\rm surv} \frac{1}{1 + \sum_{k=1}^{\Omega_{\rm occ}-1} \prod_{m=1}^{k} \widetilde{\gamma}(m)},$$

$$\theta_{\rm int}^{\rm G} = \phi_{\rm int}^{\rm G} \sum_{k=1}^{\Omega_{\rm occ}-1} \sum_{n=1}^{k} \frac{\prod_{m=n+1}^{k} \widetilde{\gamma}(m)}{\widetilde{T}_n^+} + (1 - p_{\rm surv})\tau_E, \quad \text{(F3)}$$

where

$$\widetilde{\gamma}_{\rm G}(i) \equiv \frac{\rho_W + \frac{1}{\psi-1}\frac{q_{\rm G}}{\Omega}\frac{i(\Omega_{\rm occ}-i)}{\widetilde{E}_{\rm G}(i)}}{\rho_M + \frac{1}{\psi-1}\frac{q_{\rm G}}{\Omega}\frac{i(\Omega_{\rm occ}-i)}{\widetilde{E}_{\rm G}(i)}}, \quad \text{(F4)}$$

and the upper limit of the first sum in $\phi_{\rm int}^{\rm G}$ and $\theta_{\rm int}^{\rm G}$ is rounded to the nearest integer. We find that $\phi_{\rm int}^{\rm G}$ depends on the migration rate m, carrying capacity K, and the spatial structure G via $\widetilde{\gamma}_{\rm G}$ and $\Omega_{\rm occ}$. In the case of the clique discussed in the main text, the expression of Eq. (F4) simplifies to

$$\widetilde{\gamma}_{\rm clique}(i) \equiv \widetilde{\gamma}_{\rm clique} = \frac{\rho_W + \frac{1}{\psi-1}}{\rho_M + \frac{1}{\psi-1}}. \quad \text{(F5)}$$

We notice that for all graphs G, the expressions of Eq. (F3) coincide with those of Eq. (14) of the competition-dominated regime, with $\widetilde{\gamma}_G(i) \xrightarrow{\psi \gg 1} \gamma = \rho_W/\rho_M$. In Fig. 11, we find that the predictions of Eq. (F3) are in good agreement with simulation results for all spatial structures G. Moreover, we observe that the spatial dependence of $\phi_{\rm int}^{\rm G}$ and $\theta_{\rm int}^{\rm G}$ is barely noticeable.

APPENDIX G: FIXATION PROBABILITY IN TIME-SWITCHING ENVIRONMENTS UNDER WEAK BOTTLENECKS

In this Appendix, we discuss in further detail the dependence of the fixation probability $\Phi^{\rm G}(\nu, m)$ on the migration rate m and spatial structure G of the metapopulation in time-switching environments under weak bottlenecks.

In static environments, where K is constant, a generalization of the circulation theorem guarantees that the fixation probability is independent of the migration rate and spatial structure of the metapopulation arranged on a circulation graph [see Eq. (14)]. This results from a correspondence between the fixation probability and the number of M demes performing a biased random walk on $\{0, \ldots, \Omega\}$ with a bias that is independent of m and G [41].

In time-switching environments under weak bottlenecks (deme extinction is negligible) the correspondence is between the fixation $\Phi^{\rm G}(\nu, m)$ and the random walk (with absorbing boundaries) on $\{0, \ldots, \Omega\} \times \{-1, 1\}$ for the number of fully mutant demes in the environmental state $\xi = \pm 1$. As a consequence, $\Phi^{\rm G}(\nu, m)$ is the probability of absorption in the state Ω. In this setting, defining the state of the random walk by (i, ξ), where $i = 0, 1, \ldots, \Omega$, the random walk moves to the right $(i \to i + 1)$ with a probability $r(i, \xi)$, to the left $(i \to i - 1)$ with a probability $\ell(i, \xi)$, or switches environment $(\xi \to -\xi)$ with probability $\epsilon(i, \xi)$, where

$$r(i,\xi) = \frac{m\mathcal{N}_\xi(\nu)\frac{E_{\rm G}(i)}{q_{\rm G}}\rho_{M,\xi}(\nu)}{m\mathcal{N}_\xi(\nu)\frac{E_{\rm G}(i)}{q_{\rm G}}\rho_{M,\xi}(\nu) + m\mathcal{N}_\xi(\nu)\frac{E_{\rm G}(i)}{q_{\rm G}}\rho_{W,\xi}(\nu) + \nu},$$

$$\ell(i,\xi) = \frac{m\mathcal{N}_\xi(\nu)\frac{E_{\rm G}(i)}{q_{\rm G}}\rho_{W,\xi}(\nu)}{m\mathcal{N}_\xi(\nu)\frac{E_{\rm G}(i)}{q_{\rm G}}\rho_{M,\xi}(\nu) + m\mathcal{N}_\xi(\nu)\frac{E_{\rm G}(i)}{q_{\rm G}}\rho_{W,\xi}(\nu) + \nu},$$

$$\epsilon(i,\xi) = \frac{\nu}{m\mathcal{N}_\xi(\nu)\frac{E_{\rm G}(i)}{q_{\rm G}}\rho_{M,\xi}(\nu) + m\mathcal{N}_\xi(\nu)\frac{E_{\rm G}(i)}{q_{\rm G}}\rho_{W,\xi}(\nu) + \nu}. \quad \text{(G1)}$$

$\Phi^{\rm G}(\nu, m)$ thus coincides with the probability that the random walk defined by Eq. (G1) gets absorbed in the state $i = \Omega$. Unlike the case of the competition-dominated regime under the static environment, the fixation probability here typically depends on all parameters, including the migration rate. For the fixation probability to remain unchanged under parameter changes requires strict conditions. This can be seen by assuming that for a parameter set S_1 the probabilities $r_1(i, \xi)$, $\ell_1(i, \xi)$, and $\epsilon_1(i, \xi)$ define the random walk corresponding to the fixation probability $\Phi_{i,\xi}^{\rm G}$. We therefore have

$$\Phi_{i,\xi}^{\rm G} = r_1(i,\xi)\Phi_{i+1,\xi}^{\rm G} + \ell_1(i,\xi)\Phi_{i-1,\xi}^{\rm G} + \epsilon_1(i,\xi)\Phi_{i,-\xi}^{\rm G}. \quad \text{(G2)}$$

We can also assume that under another set of parameters, say S_2, $\Phi^{\rm G}_{i,\xi}$ remains unchanged for all i and ξ with a corresponding random walk defined by the probabilities $r_2(i,\xi)$, $\ell_2(i,\xi)$, and $\epsilon_2(i,\xi)$, such that

$$\Phi^{\rm G}_{i,\xi} = r_2(i,\xi)\Phi^{\rm G}_{i+1,\xi} + \ell_2(i,\xi)\Phi^{\rm G}_{i-1,\xi} + \epsilon_2(i,\xi)\Phi^{\rm G}_{i,-\xi}. \tag{G3}$$

Subtracting the second equation from the first, and using conservation of probability, we find that

$$\begin{aligned}&(r_1(i,\xi) - r_2(i,\xi))\big(\Phi^{\rm G}_{i+1,\xi} - \Phi^{\rm G}_{i,-\xi}\big)\\ &\quad + (\ell_1(i,\xi) - \ell_2(i,\xi))\big(\Phi^{\rm G}_{i-1,\xi} - \Phi^{\rm G}_{i,-\xi}\big) = 0.\end{aligned} \tag{G4}$$

The cases of $\Phi^{\rm G}_{i+1,\xi} - \Phi^{\rm G}_{i,-\xi} = 0$ and $\Phi^{\rm G}_{i-1,\xi} - \Phi^{\rm G}_{i,-\xi} = 0$ imply that the fixation probability of all transient states is identical, and therefore we neglect this unphysical case. Defining $\Delta r(i,\xi) = r_1(i,\xi) - r_2(i,\xi)$ and $\Delta\ell(i,\xi) = \ell_1(i,\xi) - \ell_2(i,\xi)$, Eq. (G4) yields

$$\Delta r(i,\xi) = \frac{\Phi^{\rm G}_{i+1,\xi} - \Phi^{\rm G}_{i,-\xi}}{\Phi^{\rm G}_{i,-\xi} - \Phi^{\rm G}_{i-1,\xi}}\Delta\ell(i,\xi). \tag{G5}$$

For each of the $2(\Omega-2)$ transient states, we therefore have a constraint given by Eq. (G5). However, $\Delta r(i,\xi)$ and $\Delta\ell(i,\xi)$ are controlled by $|S_1| = |S_2| = p$ degrees of freedom (system parameters) where $p \ll 2(\Omega-2)$. Therefore, the system is overdetermined and Eq. (G5) is only generally satisfied across all (i,ξ) for the trivial solution $\Delta r(i,\xi) = \Delta\ell(i,\xi) = 0$, i.e., $S_1 = S_2$. Thus, in time-fluctuating environments, the fixation probability $\Phi^{\rm G}(\nu,m)$ is expected to depend on m and G.

Interestingly, however, Fig. 4(c) illustrates the almost unnoticeable dependence of $\Phi^{\rm G}(\nu,m)$ on the specific spatial structure. This is due to the overall similar impact of the factor $E_{\rm G}(i)/q_G$ for the various graphs. While differences arise when m varies at fixed ν due to large variations in the timescales of the competition dynamics, varying spatial structure produces small changes in these timescales, and as such leads to only unnoticeable changes in $\Phi^{\rm G}$.

APPENDIX H: ASYMMETRIC DICHOTOMOUS MARKOV NOISE AND ENVIRONMENTAL BIAS

For the sake of simplicity and clarity, in the main text we have focused on symmetric environmental switching. In this Appendix, we relax this assumption and outline how the results of the paper can be generalized to the case when there is an environmental bias, i.e., when there is a different average time spent in the states $\xi = \pm 1$.

Here, we consider the colored asymmetric dichotomous Markov noise (aDMN), also called telegraph process, $\xi(t) \in \{-1,1\}$ that switches between ±1 according to $\xi \to -\xi$ at rate $\nu_\pm$ when $\xi = \pm1$ [69–71]. It is convenient to write these asymmetric switching rates as $\nu_\pm = \nu(1 \mp \delta)$, where $\nu \equiv (\nu_- + \nu_+)/2$ is the mean switching rate, and $\delta \equiv (\nu_- - \nu_+)/(\nu_- + \nu_+) = (\nu_- - \nu_+)/(2\nu)$ denotes the switching bias, with $|\delta| \leqslant 1$ and $\delta > 0$ when more time is spent on average in the mild environment [18,19]. At stationarity, this aDMN has average $\langle\xi(t)\rangle = \delta$ and autocovariance $\langle\xi(t)\xi(t')\rangle - \langle\xi(t)\rangle\langle\xi(t')\rangle = (1-\delta^2)e^{-2\nu|t-t'|}$ [16,17,69–71].

The aDMN drives the *time-switching* carrying capacity

$$K(t) = \tfrac{1}{2}[K_+ + K_- + \xi(t)(K_+ - K_-)], \tag{H1}$$

which is the same expression as Eq. (6), but now driven by the aDMN $\xi(t)$ [16–19,21,22,32]. The carrying capacity switches back and forth between K_+ (mild environment, $\xi = +1$) and $K_- < K_+$ (harsh environment, $\xi = -1$) at rates $\nu_\pm = \nu(1 \mp \delta)$ according to

$$K_+ \underset{\nu_-}{\overset{\nu_+}{\rightleftharpoons}} K_-.$$

At stationarity, the expected value of the carrying capacity is $\langle K(t)\rangle = \frac{1}{2}(K_+ + K_- + \delta(K_+ - K_-))$, and its autocovariance is $\langle K(t)K(t')\rangle - \langle K(t)\rangle\langle K(t')\rangle = (\frac{K_+-K_-}{2})^2(1-\delta^2)e^{-2\nu|t-t'|}$ [69–71]. Under asymmetric switching, the stationary population distribution of a single deme is well approximated by the stationary density of the piecewise Markov process [Eq. (A3)] (n-PDMP) [17], now driven by the aDMN, whose joint density is

$$p_\xi(n;\nu,\delta) \propto \begin{cases} \frac{1+\delta}{n^2}\left(\frac{K_+-n}{n}\right)^{\nu(1-\delta)-1}\left(\frac{n-K_-}{n}\right)^{\nu(1+\delta)} & \text{if } \xi = +1,\\ \frac{1-\delta}{n^2}\left(\frac{K_+-n}{n}\right)^{\nu(1-\delta)}\left(\frac{n-K_-}{n}\right)^{\nu(1+\delta)-1} & \text{if } \xi = -1,\end{cases} \tag{H2}$$

where the proportional factor accounts for the normalization constants. The stationary marginal density of this n-PDMP, up to the normalization constant, is

$$\begin{aligned}p(n;\nu,\delta) &= \sum_\xi \left(\frac{1+\xi\delta}{2}\right)p_\xi(n;\nu,\delta)\\ &\propto \frac{1}{n^2}\left(\frac{K_+-n}{n}\right)^{\nu(1-\delta)-1}\left(\frac{n-K_-}{n}\right)^{\nu(1+\delta)-1},\end{aligned} \tag{H3}$$

where we have again omitted the normalization constant. The n-PDMP density captures the mean features of the deme size distribution: It is bimodal with peaks at K_+ and K_- ($n \approx K_\pm$) when $\nu \ll 1$, and is unimodal and centered around $n \approx 2K_+K_-/[(1-\delta)K_+ + (1+\delta)K_-]$ when $\nu \gg 1$ [18,21,22,24,32]. When $\nu(1\pm\delta) \lesssim 1$, the size n of each deme tracks the carrying capacity, and a bottleneck occurs at an average frequency $\nu_+\nu_-/(2\nu) = \nu(1-\delta^2)/2$, each time K switches from K_+ to K_- [18,21,32].

In the realm of the coarse-grained description discussed in the main text, the regime of weak bottlenecks dominated by the W/M competition can be characterized by the M fixation probability $\Phi^{\rm G}(\nu,\delta,m)$ and unconditional mean fixation time $\Theta^{\rm G}(\nu,\delta,m)$ by Eq. (26) obtained by solving the first-step analysis equations [Eqs. (23) and (24)] with the transition rates [Eqs. (21) and (22)] obtained using $N_\xi(\nu,\delta)$ averaged over Eq. (H3), i.e., $N_\xi(\nu,\delta) = \int np_\xi(n;\nu,\delta)\mathrm{d}n$. The results of Fig. 12 for a clique metapopulation show that the predictions of the coarse-grained description based on the PDMP approximation [Eq. (H3)] are in good agreement with simulation results. $\Phi^{\rm G}(\nu,\delta,m)$ and $\Theta^{\rm G}(\nu,\delta,m)$ are again found to exhibit a nonmonotonic dependence on ν, with extrema in the range of intermediate ν. The main effect of δ is to increase the M fixation probability and reduce the mean fixation time when $\delta > 0$, which is intuitively clear since this corresponds to a bias toward the mild state favoring the fixation of M.

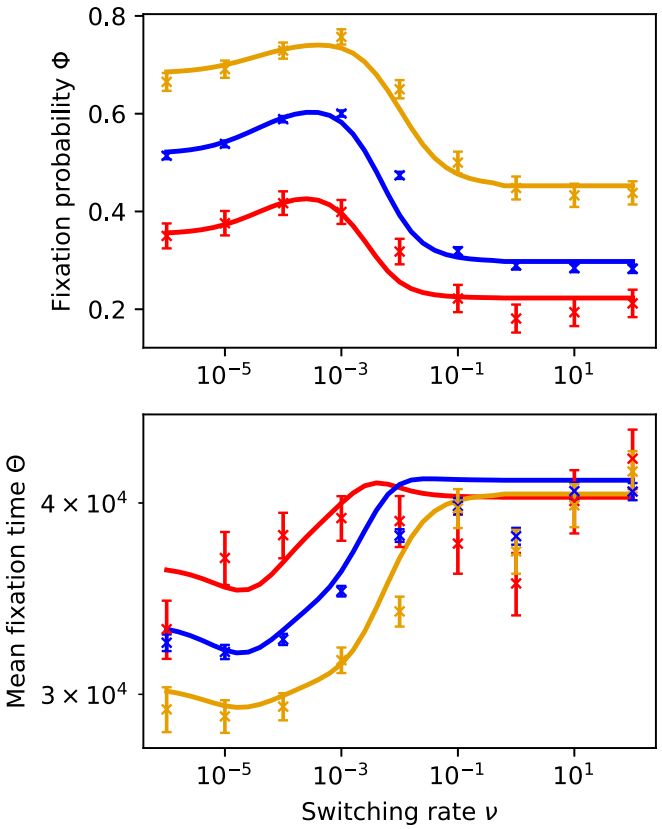

FIG. 12. Fixation probability Φ^{G} and mean fixation time Θ^{G} against switching rate ν for different values of δ for a clique metapopulation. Red, blue, and yellow represent $\delta = -0.5$, $\delta = 0.0$, and $\delta = 0.5$, respectively. Markers show simulation results and lines are predictions of Eq. (26). Other parameters are $\Omega = 16$, $s = 0.01$, $m = 10^{-4}$, $K_+ = 200$, and $K_- = 20$.

The regime of strong bottlenecks is dominated by the interplay between M/W competition in the mild state ($K = K_+$) and deme extinction in the harsh environmental state ($K = K_-$), occurring in time $\theta_E \equiv \theta_E(K_-, \Omega)$. In this regime, the near-optimal conditions for the removal of the mutant strain can be obtained as under symmetric switching [given by Eq. (27)] and read

$$\psi(m, K_-) < 1, \qquad \nu(1 \pm \delta) \lesssim 1,$$
$$\nu(1+\delta)\theta_E \gtrsim 1, \qquad mK_+\theta_E \frac{1+\delta}{1-\delta} \gtrsim 1, \tag{H4}$$

which, as Eq. (27), are conditions depending on m but not on the spatial structure G. The main differences from Eq. (27) are in the conditions $\theta_E \nu_- = \theta_E \nu(1+\delta) \gtrsim 1$ and $mK_+\theta_E \frac{\nu_-}{\nu_+} = mK_+\theta_E \frac{1+\delta}{1-\delta} \gtrsim 1$. The first of these changes ensures that a switch occurs before the metapopulation mean extinction time in the harsh environment, θ_E. The second ensures there are enough recolonizations in the mild environment to maintain the metapopulation given the minimum switching rate required to prevent extinction in the harsh environment, i.e., rearranging $\theta_E \nu_- \gtrsim 1$ gives $\nu \gtrsim 1/(\theta_E(1+\delta))$ and for sufficient recolonizations we require $mK_+/\nu_+ \equiv mK_+/(\nu(1-\delta)) \gtrsim 1$, where we substitute our expression for ν. Since θ_E is independent of δ, we expect that the conditions [Eq. (H4)] define a region in the parameter space that is similar to that obtained under symmetric switching, shifted toward higher (lower) values of ν and K_- when $\delta < 0$ ($\delta > 0$). This picture is confirmed by the heatmaps of Fig. 13.

APPENDIX I: SIMULATION METHODS AND PLOTS

In this Appendix, we explain how the simulation of the individual-based dynamics of the full model has been implemented. We also outline how we have plotted the simulation/numerical data that we have obtained to produce the figures discussed in the main text and Appendixes.

In addition to the coarse-grained descriptions of the model that provide us with analytical approximations of metapopulation dynamics in different regimes, we have employed Monte Carlo (MC) methods to simulate the full individual-based model and mirror the dynamics encoded in the ME of Eq. (A1). In this section, we outline how we have performed the stochastic simulations that we have notably used to test our analytical predictions.

While not exact like other simulation methods (e.g., the Gillespie algorithm [98]) due to time discretization, the MC algorithm used here improves on computational efficiency making simulations with larger numbers of cells on the metapopulation that run for long times feasible and straightforward to implement. The questions of computational efficiency and tractability are particularly critical in the context of this work in which we study fixation and extinction of spatially arranged populations, a notoriously computationally demanding problem. In this context, MC algorithms similar to the one used are useful tools to investigate the properties of spatially extended systems (see, for example, Ref. [99].

In the case of symmetric environmental switching, the MC algorithm that we have employed can be described as follows: The graph, consisting of the spatially arranged Ω deme forming the metapopulation, is initialized by randomly picking an initial value for the carrying capacity $K(0) = \{K_-, K_+\}$ with equal probability [in the constant environment case $K(0) = K$ with probability 1], populating a single deme with $K(0)$ M cells, and the remaining $\Omega - 1$ of the demes with $K(0)$ W cells. Time is then discretized in units of Monte Carlo steps (MCS) whereby in each MCS we perform $2N$ birth-death events, where N is measured at the start of the MCS. We choose $2N$ as we typically have N births and N deaths per unit time according to the transition rates [Eqs. (2) and (4)] when summing over all cells on the metapopulation. Therefore, our units of time are consistent between the theoretical model and the Monte Carlo simulation. We emphasize that migration events and environmental switches do not contribute to the $2N$ events comprising an MCS. Therefore, $2N$ birth-death events are performed in a single MCS, and the expected number of migrations and environmental switches in the MCS corresponds to the migration and switching events expected in one unit of time. Each of the $2N$ events in an MCS occurs sequentially and the rates are updated for the next event in the MCS. The type of each event in an MCS is selected sequentially based on the rates of the events, where a higher rate means a larger probability of that event being selected. Concretely, the following steps for a single MCS occur:

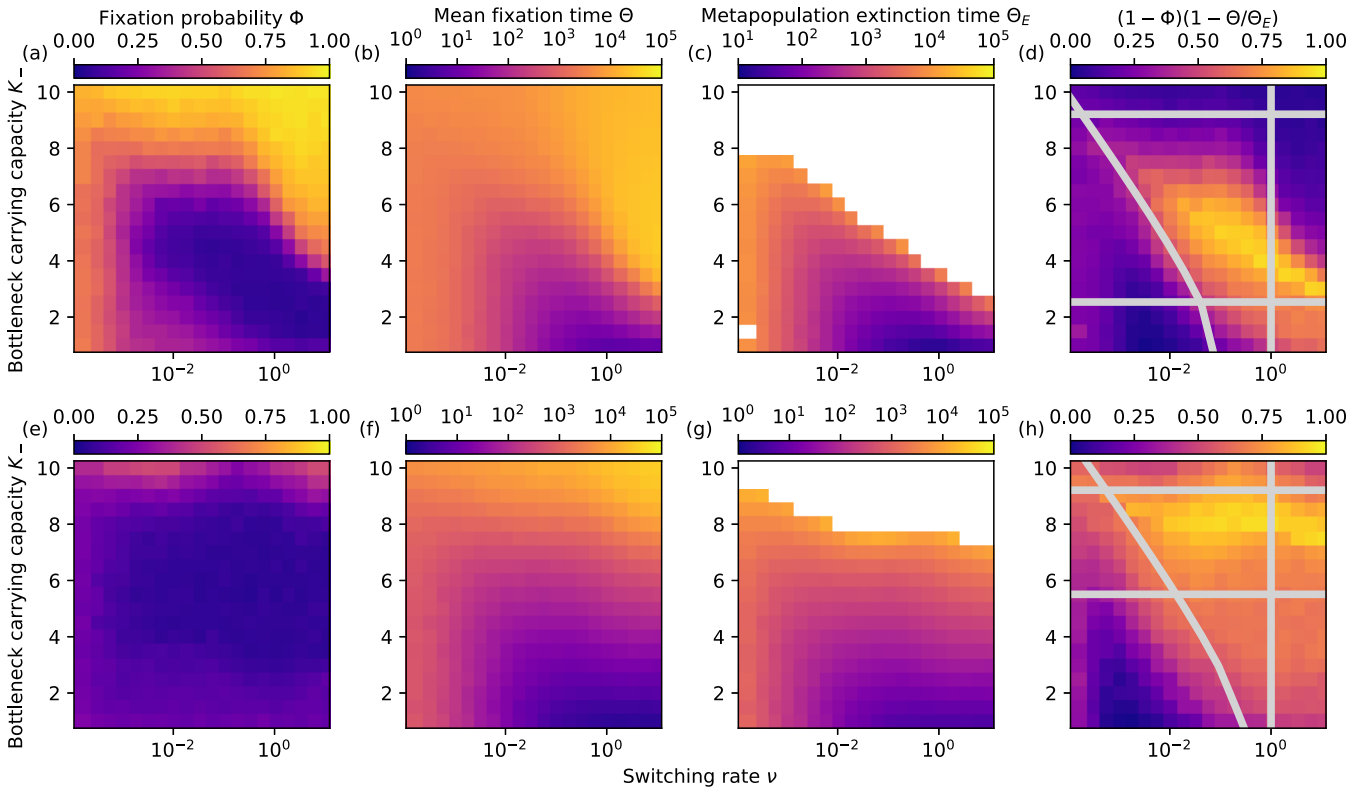

FIG. 13. Near-optimal condition for the idealized treatment strategy on the clique metapopulation. (ν, K_-) heatmaps of Φ, Θ, Θ_E and $(1-\Phi)(1-\Theta/\Theta_E)$ for (a)–(d) $\delta = 0.5$ and (e)–(h) $\delta = -0.5$ metapopulations (see Appendix H). Whitespace in panels (c) and (g) indicate the region of the parameter where at least one realization for those parameters did not reach extinction by $t = 10^5$. Gray lines in panels (d) and (h) show the near-optimal conditions for the idealized treatment strategy in the asymmetric environment: $\psi(m, K_-) < 1$ below the top horizontal line, $mK_+\theta_E \frac{1+\delta}{1-\delta} > 1$ above the bottom horizontal line, and $\nu(1+\delta)\theta_E > 1$ above the curved line, while the vertical line indicates where $\nu < 1$ and θ_E from Eq. (15). The near-optimal treatment conditions is the yellowish cloud at the center of the area enclosed by these lines. Other parameters are $\Omega = 16$, $m = 10^{-4}$, $s = 0.1$, and $K_+ = 200$. In all panels, initially there is a single M deme and $\Omega - 1$ demes occupied by W.

(1) Check if an environmental switch, occurring with rate ν, occurs on the metapopulation. The rate of reaction of birth-death-migration events on the entire metapopulation is $N(1 + m + N/K(t))$. Therefore, the probability of an environmental switch is given by $\nu/(N(1 + m + N/K(t)) + \nu)$.

(2) Otherwise, a deme x is picked for an event to occur based on the total rate of events on that deme, $n(x)(1 + m + n(x)/K(t))$. Therefore, the probability of selecting a deme x for an event is $\frac{n(x)(1+m+n(x)/K(t))}{N(1+m+N/K(t))}$.

(3) A species is picked for an event to occur based on the total rate of events of that species on the selected deme. The propensity of a given species α on deme x is $n_\alpha(x)(1 + m + n(x)/K(t))$, and the total rate of events on the deme is as in the previous step. Therefore, that species is selected with probability $\frac{n_\alpha(x)(1+m+n(x)/K(t))}{n(x)(1+m+n(x)/K(t))} = \frac{n_\alpha(x)}{n(x)}$.

(4) The species on the deme can then either undergo a birth, death, or migration event, with the probability of each depending on the rates of these events. Birth, death, or migration is selected with probability $\frac{T_\alpha^{+,-,m}(x)}{n_\alpha(x)(1+m+n(x)/K(t))}$.

(5) The selected event is performed.

(6) The above steps are repeated until $2N$ birth-death events are performed.

Each event is selected based on the current propensities of the system, and those are subsequently updated before the selection of the next event. The probability of events in our MC algorithm is thus statistically equivalent to that of a simulation generating the statistically correct sample paths (e.g., Gillespie [98]). The approximation of this algorithm is to assign each MCS to $2N$ birth-death events with N defined at the start of the MCS, unlike a statistically exact simulation algorithm where each event time is drawn individually.

In all simulations, each realization is simulated until fixation, tracking when fixation occurs and which species fixates. In simulations for Figs. 2(b), 6, 10, and 13, the simulation then continues until metapopulation extinction or a large fixed time T (here we set $T = 10^5$). For a given set of parameters, if extinction does not occur in any realization, the extinction time is not recorded. The data are averaged to obtain the fixation probability, the mean fixation time, and the mean time to extinction where applicable. Furthermore, we record the standard error on the mean for each quantity. In Figs. 2, 4, and 12, 10^3 realizations are ran for each set of parameters, and these data are plotted with the standard error on the mean shows as error bars. In the heatmaps, each data point corresponds to the

average value for 10^3 simulations at that point in parameter space. The standard error on the mean is not plotted for the heatmaps.

In the case that $K(t) = K =$ constant, we set $\nu = 0$ and $K_+ = K_- = K$, such that the first step of the above process is effectively skipped. In the case that the switching is asymmetric, the starting state is chosen according to the stationary distribution of $K(t)$, i.e., $K(0) = K_\pm$ with probability $\frac{1\pm\delta}{2}$. The probability for an environmental switch in the first step then depends on the current environmental state, where a switch occurs with probability $\nu_\pm/(N(1 + m + N/K(t) + \nu_\pm)$ for $K(t) = K_\pm$.

[1] S. Widder *et al.*, Challenges in microbial ecology: Building predictive understanding of community function and dynamics, ISME J. **10**, 2557 (2016).

[2] P. Engel and N. Moran, The gut microbiota of insects–diversity in structure and function, FEMS Microbiol. Rev. **37**, 699 (2013).

[3] N. Garud, B. Good, O. Hallatschek, and K. Pollard, Evolutionary dynamics of bacteria in the gut microbiome within and across hosts, PLoS Biol. **17**, e3000102 (2019).

[4] J. J. She *et al.*, Defining the biogeographical map and potential bacterial translocation of microbiome in human surface organs, Nat. Commun. **15**, 427 (2024).

[5] F. Cignarella *et al.*, Intermittent fasting confers protection in cns autoimmunity by altering the gut microbiota, Cell Metab. **27**, 1222 (2018).

[6] S. A. Smits *et al.*, Seasonal cycling in the gut microbiome of the Hadza hunter-gatherers of Tanzania, Science **357**, 802 (2017).

[7] W. Ewens, *Mathematical Population Genetics* (Springer, New York, 2004).

[8] J. F. Crow and M. Kimura, *An Introduction to Population Genetics Theory* (Blackburn Press, Caldwell, NJ, 2009).

[9] J. Roughgarden, *Theory of Population Genetics and Evolutionary Ecology: An Introduction* (Macmillan, New York, 1979).

[10] A. Melbinger, J. Cremer, and E. Frey, Evolutionary game theory in growing populations, Phys. Rev. Lett. **105**, 178101 (2010).

[11] J. Cremer, A. Melbinger, and E. Frey, Frey, evolutionary and population dynamics: A coupled approach, Phys. Rev. E **84**, 051921 (2011).

[12] J. Cremer, A. Melbinger, and E. Frey, Growth dynamics and the evolution of cooperation in microbial populations, Sci. Rep. **2**, 281 (2012).

[13] A. Melbinger, J. Cremer, and E. Frey, The emergence of cooperation from a single mutant during microbial life cycles, J. R. Soc. Interface **12**, 20150171 (2015).

[14] J. S. Chuang, O. Rivoire, and S. Leibler, Simpson's paradox in a synthetic microbial system, Science **323**, 272 (2009).

[15] N. Verdon, O. Popescu, S. Titmuss, and R. J. Allen, Habitat fragmentation enhances microbial collective defence, J. R. Soc. Interface **22**, 20240611 (2025).

[16] K. Wienand, E. Frey, and M. Mobilia, Evolution of a fluctuating population in a randomly switching environment, Phys. Rev. Lett. **119**, 158301 (2017).

[17] K. Wienand, E. Frey, and M. Mobilia, Eco-evolutionary dynamics of a population with randomly switching carrying capacity, J. R. Soc. Interface **15**, 20180343 (2018).

[18] A. Taitelbaum, R. West, M. Assaf, and M. Mobilia, Population dynamics in a changing environment: Random versus periodic switching, Phys. Rev. Lett. **125**, 048105 (2020).

[19] A. Taitelbaum, R. West, M. Mobilia, and M. Assaf, Evolutionary dynamics in a varying environment: Continuous versus discrete noise, Phys. Rev. Res. **5**, L022004 (2023).

[20] S. Shibasaki, M. Mobilia, and S. Mitri, Exclusion of the fittest predicts microbial community diversity in fluctuating environments, J. R. Soc. Interface **18**, 20210613 (2021).

[21] L. Hernández-Navarro, M. Asker, A. M. Rucklidge, and M. Mobilia, Coupled environmental and demographic fluctuations shape the evolution of cooperative antimicrobial resistance, J. R. Soc. Interface **20**, 20230393 (2023).

[22] M. Asker, L. Hernández-Navarro, A. M. Rucklidge, and M. Mobilia, Coexistence of competing microbial strains under twofold environmental variability and demographic fluctuations, New J. Phys. **25**, 123010 (2023).

[23] R. West and M. Mobilia, Fixation properties of rock-paper-scissors games in fluctuating populations, J. Theor. Biol. **491**, 110135 (2020).

[24] L. Hernández-Navarro, M. Asker, and M. Mobilia, Eco-evolutionary dynamics of cooperative antimicrobial resistance in a population of fluctuating volume and size, J. Phys. A: Math. Theor. **57**, 265003 (2024).

[25] L. M. Wahl, P. J. Gerrish, and I. Saika-Voivod, Evaluating the impact of population bottlenecks in experimental evolution, Genetics **162**, 961 (2002).

[26] P. B. Rainey and K. Rainey, Evolution of cooperation and conflict in experimental bacterial populations, Nature (London) **425**, 72 (2003).

[27] Z. Patwa and L. M. Wahl, Adaptation rates of lytic viruses depend critically on whether host cells survive the bottleneck, Evolution **64**, 1166 (2010).

[28] M. A. Brockhurst, A. Buckling, and A. Gardner, Cooperation peaks at intermediate disturbance, Curr. Biol. **17**, 761 (2007).

[29] M. A. Brockhurst, Population bottlenecks promote cooperation in bacterial biofilms, PLoS One **2**, e634 (2007).

[30] J. Coates, B. R. Park, D. Le, E. Şimşek, W. Chaudhry, and M. Kim, Antibiotic-induced population fluctuations and stochastic clearance of bacteria, eLife **7**, e32976 (2018).

[31] N. Mahrt, A. Tietze, S. Künzel, S. Franzenburg, C. Barbosa, G. Jansen, and H. Schulenburg, Bottleneck size and selection level reproducibly impact evolution of antibiotic resistance, Nat. Ecol. Evol. **5**, 1233 (2021).

[32] L. Hernández-Navarro, K. Distefano, U. C. Täuber, and M. Mobilia, Slow spatial migration can help eradicate cooperative antimicrobial resistance in time-varying environments, bioRxiv (2025).

[33] S. Wright, Evolution in Mendelian populations, Genetics **16**, 97 (1931).

[34] M. Kimura and G. H. Weiss, The stepping stone model of population structure and the decrease of genetic correlation with distance, Genetics **49**, 561 (1964).

[35] R. Levins, Some demographic and genetic consequences of environmental heterogeneity for biological control, Bull. Entomol. Soc. Am. **15**, 237 (1969).

[36] I. Hanski, *Metapopulation Ecology* (Oxford University Press, New York, 1999).
[37] C. Lugo and A. J. McKane, Quasicycles in a spatial predator-prey model, Phys. Rev. E **78**, 051911 (2008).
[38] T. Butler and N. Goldenfeld, Robust ecological pattern formation induced by demographic noise, Phys. Rev. E **80**, 030902(R) (2009).
[39] B. Szczesny, M. Mobilia, and A. M. Rucklidge, Characterization of spiraling patterns in spatial rock-paper-scissors games, Phys. Rev. E **90**, 032704 (2014).
[40] F. Peruzzo, M. Mobilia, and S. Azaele, Spatial patterns emerging from a stochastic process near criticality, Phys. Rev. X **10**, 011032 (2020).
[41] L. Marrec, I. Lamberti, and A.-F. Bitbol, Toward a universal model for spatially structured populations, Phys. Rev. Lett. **127**, 218102 (2021).
[42] A. Moawad, A. Abbara, and A.-F. Bitbol, Evolution of cooperation in deme-structured populations on graphs, Phys. Rev. E **109**, 024307 (2024).
[43] T. Maruyama, On the fixation probability of mutant genes in a subdivided population, Genet. Res. **15**, 221 (1970).
[44] N. Barton, The probability of fixation of a favoured allele in a subdivided population, Genet. Res. **62**, 149 (1993).
[45] M. C. Whitlock and N. H. Barton, The effective size of a subdivided population, Genetics **146**, 427 (1997).
[46] M. C. Whitlock, Fixation probability and time in subdivided populations, Genetics **164**, 767 (2003).
[47] E. Lieberman, C. Hauert, and M. A. Nowak, Evolutionary dynamics on graphs, Nature (London) **433**, 312 (2005).
[48] B. Houchmandzadeh and M. Vallade, The fixation probability of a beneficial mutation in a geographically structured population, New J. Phys. **13**, 073020 (2011).
[49] B. Allen, G. Lippner, Y.-T. Chen, B. Fotouhi, N. Momeni, S.-T. Yau, and M. A. Nowak, Evolutionary dynamics on any population structure, Nature (London) **544**, 227 (2017).
[50] A. Abbara and A.-F. Bitbol, Frequent asymmetric migrations suppress natural selection in spatially structured populations, PNAS Nexus **2**, pgad392 (2023).
[51] L. Marrec, Quantifying the impact of genotype-dependent gene flow on mutation fixation in subdivided populations, bioRxiv (2023).
[52] S. Yagoobi and A. Traulsen, Fixation probabilities in network structured meta-populations, Sci. Rep. **11**, 17979 (2021).
[53] J. Tkadlec, K. Kaveh, K. Chatterjee, and M. A. Nowak, Evolutionary dynamics of mutants that modify population structure, J. R. Soc. Interface **20**, 20230355 (2023).
[54] A. Abbara, L. Pagani, C. García-Pareja, and A.-F. Bitbol, Mutant fate in spatially structured populations on graphs: Connecting models to experiments, PLoS Comput. Biol. **20**, e1012424 (2024).
[55] S. Kryazhimskiy, D. P. Rice, and M. M. Desai, Population subdivision and adaptation in asexual populations of *Saccharomyces cerevisiae*, Evolution **66**, 1931 (2012).
[56] J. R. Nahum, P. Godfrey-Smith, B. N. Harding, J. H. Marcus, J. Carlson-Stevermer, and B. Kerr, A tortoise-hare pattern seen in adapting structured and unstructured populations suggests a rugged fitness landscape in bacteria, Proc. Natl. Acad. Sci. USA **112**, 7530 (2015).
[57] P. P. Chakraborty, L. R. Nemzer, and R. Kassen, Experimental evidence that network topology can accelerate the spread of beneficial mutations, Evol. Lett. **7**, 447 (2023).
[58] J. Kreger, D. Brown, N. L. Komarova, D. Wodarz, and J. Pritchard, The role of migration in mutant dynamics in fragmented populations, J. Evol. Biol. **36**, 444 (2023).
[59] R. Lande, S. Engen, B.-E. Sæther, and B.-E. Saether, Extinction times in finite metapopulation models with stochastic local dynamics, Oikos **83**, 383 (1998).
[60] C. Fruet, E. L. Müller, C. Loverdo, and A.-F. Bitbol, Spatial structure facilitates evolutionary rescue by drug resistance, PLoS Comput. Biol. **21**, e1012861 (2025).
[61] S. Wright, Isolation by distance, Genetics **28**, 114 (1943).
[62] S. Wright, Population structure in evolution, Proc. Am. Philos. Soc. 93, 471 (1949).
[63] J. E. Keymer, P. Galajda, C. Muldoon, S. Park, and R. H. Austin, Bacterial metapopulations in nanofabricated landscapes, Proc. Natl. Acad. Sci. USA **103**, 17290 (2006).
[64] P. Moran, *The Statistical Processes of Evolutionary Theory* (Clarendon Press, Oxford, 1962).
[65] R. Blythe and A. McKane, Stochastic models of evolution in genetics, ecology and linguistics, J. Stat. Mech. (2007) P07018.
[66] A. Traulsen and C. Hauert, Stochastic evolutionary game dynamics, in *Reviews of Nonlinear Dynamics and Complexity*, edited by H. G. Schuster (Wiley-VCH, Weinheim, Germany, 2009), Vol. 2, pp. 25–61.
[67] T. Antal and I. Scheuring, Fixation of strategies for an evolutionary game in finite populations, Bull. Math. Biol. **68**, 1923 (2006).
[68] Here, we use the growth of the M cluster to define slow migration as the mutant has a fitness advantage. Therefore, $\rho_M > \rho_W$ and $T_i^+(m, \mathrm{G}, K) > T_i^-(m, \mathrm{G}, K)$ in general.
[69] I. Bena, Dichotomous Markov Noise: Exact results for out-of-equilibrium systems, Int. J. Mod. Phys. B **20**, 2825 (2006).
[70] W. Horsthemke and R. Lefever, *Noise-Induced Transitions* (Springer, Berlin, 2006).
[71] L. Ridolfi, P. D'Odorico, and F. Laio, *Noise-Induced Phenomena in the Envionmental Sciences* (Cambridge University Press, Cambridge, 2011).
[72] C. W. Gardiner, *Handbook of Stochastic Methods* (Springer, Berlin, Germany, 2002).
[73] L. J. S. Allen, *An Introduction to Stochastic Processes with Applications to Biology*, 1st ed. (Pearson Education, 2003).
[74] L. Witting, J. Seiffarth, B. Stute, T. Schulze, J. M. Hofer, K. Nöh, M. Eisenhut, A. P. M. Weber, E. von Lieres, and D. Kohlheyer, A microfluidic system for the cultivation of cyanobacteria with precise light intensity and CO_2 control: Enabling growth data acquisition at single-cell resolution, Lab Chip **25**, 319 (2025).
[75] A. Rodríguez-Verdugo, C. Vulin, and M. Ackermann, The rate of environmental fluctuations shapes ecological dynamics in a two-species microbial system, Ecol. Lett. **22**, 838 (2019).
[76] R. Hengge-Aronis, Survival of hunger and stress: The role of *rpoS* in early stationary phase gene regulation in *E. coli*, Cell **72**, 165 (1993).
[77] C. R. Morley, J. A. Trofymow, D. C. Coleman, and C. Cambardella, Effects of freeze-thaw stress on bacterial populations in soil microcosms, Microb. Ecol. **9**, 329 (1983).

[78] F. Vasi, M. Travisano, and R. E. Lenski, Long-term experimental evolution in *Escherichia coli*. II. changes in life-history traits during adaptation to a seasonal environment, Am. Nat. **144**, 432 (1994).

[79] C. A. Fux, J. W. Costerton, P. S. Stewart, and P. Stoodley, Survival strategies of infectious biofilms, Trends Microbiol. **13**, 34 (2005).

[80] M. Acar, J. T. Mettetal, and A. van Oudenaarden, Stochastic switching as a survival strategy in fluctuating environments, Nat. Genet. **40**, 471 (2008).

[81] T. Proft, *Microbial Toxins: Current Research and Future Trends* (Caister Academic Press, Norfolk, UK, 2009).

[82] J. G. Caporaso, C. L. Lauber, E. K. Costello, D. Berg-Lyons, A. Gonzalez, J. Stombaugh, D. Knights, P. Gajer, J. Ravel, N. Fierer, J. I. Gordon, and R. Knight, Moving pictures of the human microbiome, Genome Biol. **12**, R50 (2011).

[83] Y. Himeoka and N. Mitarai, Dynamics of bacterial populations under the feast-famine cycles, Phys. Rev. Res. **2**, 013372 (2020).

[84] P. Tu, L. Chi, W. Bodnar, Z. Zhang, B. Gao, X. Bian, J. Stewart, R. Fry, and K. Lu, Gut microbiome toxicity: Connecting the environment and gut microbiome-associated diseases, Toxics **8**, 19 (2020).

[85] M. H. A. Davis, Piecewise-deterministic Markov processes: A general class of non-diffusion Stochastic models, J. R. Stat. Soc. Ser. B Methodol. **46**, 353 (1984).

[86] P. Hufton, Y. T. Lin, T. Galla, and M. A. J, Intrinsic noise in systems with switching environments, Phys. Rev. E **93**, 052119 (2016).

[87] M. Slatkin, Fixation probabilities and fixation times in a subdivided population, Evolution **35**, 477 (1981).

[88] P. L. Krapivsky, S. Redner, and E. Ben-Naim, *A Kinetic View of Statistical Physics* (Cambridge University Press, Cambridge, 2010).

[89] U. C. Täuber, *Critical Dynamics* (Cambridge University Press, Cambridge, 2014).

[90] K. Totlani, J.-W. Hurkmans, W. M. van Gulik, M. T. Kreutzer, and V. van Steijn, Scalable microfluidic droplet on-demand generator for non-steady operation of droplet-based assays, Lab Chip **20**, 1398 (2020).

[91] R. H. Hsu, R. L. Clark, J. W. Tan, J. C. Ahn, S. Gupta, P. A. Romero, and O. S. Venturelli, Microbial interaction network inference in microfluidic droplets, Cell Syst. **9**, 229 (2019).

[92] S. Ganchua, A. White, E. Klein, and J. Flynn, Lymph nodes–the neglected battlefield in tuberculosis, PLoS Pathog. **16**, e1008632 (2020).

[93] W. Van den Broeck, A. Derore, and P. Simoens, Anatomy and nomenclature of murine lymph nodes: Descriptive study and nomenclatory standardization in BALB/cAnNCrl mice, J. Immunol. Methods **312**, 12 (2006).

[94] G. Lambert and E. Kussell, Memory and fintess optimization of bacteria under fluctuating environments, PLoS Genet. **10**, e1004556 (2014).

[95] F. Abdul-Rahman, D. Tranchina, and D. Gresham, Fluctuating environments maintain genetic diversity through neutral fitness effects and balancing selection, Mol. Biol. Evol. **38**, 4362 (2021).

[96] https://eedfp.com.

[97] M. Asker, M. Swailem, U. C. Täuber, and M. Mobilia, Dataset for 'Fixation and extinction in time-fluctuating spatially structured metapopulations', University of Leeds [Dataset], Zenodo (2025), https://doi.org/10.5518/1660.

[98] D. T. Gillespie, A general method for numerically simulating the stochastic time evolution of coupled chemical reactions, J. Comput. Phys. **22**, 403 (1976).

[99] U. Dobramysl, M. Mobilia, M. Pleimling, and U. C. Täuber, Stochastic population dynamics in spatially extended predator–prey systems, J. Phys. A: Math. Theor. **51**, 063001 (2018).